A STUDY ON CHARACTERISTICS OF A QUASI-OPTICAL ANTENNA-MIXER AND ITS APPLICATIONS

SUWAN JANIN

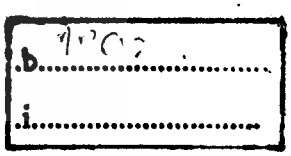

A THESIS SUBMITTED IN PARTIAL FULFILLMENT OF THE REQUIREMENT FOR THE DEGREE OF DOCTOR OF ENGINEERING IN ELECTRICAL ENGINEERING SCHOOL OF GRADUATE STUDIES KING MONGKUT'S INSTITUTE OF TECHNOLOGY LADKRABANG

2008

KMITL-2008-EN-D-018-191

หัวข้อวิทยานิพนธ์	การศึกษาลักษณะสมบัติและการประยุกต์ใช้งานสายอากาศผสมสัญญาณแบบหลักการกึ่งแสง
นักศึกษา	นายสุวรรณ จันทร์อินทร์
รหัสนักศึกษา	47060002
ปริญญา	วิศวกรรมศาสตรดุษฎีบัณฑิต
สาขาวิชา	วิศวกรรมไฟฟ้า
พ.ศ.	2551
อาจารย์ผู้ควบคุมวิทยานิพนธ์	ศ.ดร.โมไนย ไกรฤกษ์
อาจารย์ผู้ควบคุมวิทยานิพนธ์ร่วม	ดร.เกียรติศักดิ์ ศรีพิมานวัฒน์

บทคัดย่อ

วิทยานิพนธ์เล่มนี้ได้กล่าวถึงการศึกษาหลักการของสายอากาศผสมสัญญาณแบบหลักการกึ่งแสง และการประยุกต์ใช้งาน ทฤษฎีพื้นฐานของสายอากาศผสมสัญญาณแบบหลักการกึ่งแสงและสมการปรับลำคลื่นได้ถูกวิเคราะห์และแสดงตัวอย่างเพื่อความเข้าใจหลักของสายอากาศ ลำดับการศึกษาเริ่มจากสายอากาศผสมสัญญาณโดยใช้สายอากาศผสมสัญญาณหลักการกึ่งแสงวงแหวนแบบไฮบริด ลำดับต่อมาเป็นการออกแบบส่วนประกอบของสายอากาศซึ่งประกอบด้วยสายอากาศผสมสัญญาณแบบหลักการกึ่งแสงวงแหวนแบบไฮบริด ผลการทดสอบคุณสมบัติในแถบความถี่ K สายอากาศองค์ประกอบเป็นสายอากาศแบบแผ่นสี่เหลี่ยมจัตุรัสเชื่อมต่อผ่านช่องว่างแบบหลังชนกัน ทำหน้าที่รับสัญญาณความถี่วิทยุที่ความถี่ 18.8 GHz ส่งผ่านไปยังพอร์ทซิกม่าของตัวผสมสัญญาณวงแหวนแบบไฮบริดขณะที่อีกด้านหนึ่งรับสัญญาณออสซิลเลเตอร์ประจำเครื่องที่ความถี่ 17.5 GHz ส่งผ่านไปยังพอร์ทเดลต้า ไดโอดซอร์ตกี้ HSCH-9101 ทำหน้าที่แปลงสัญญาณความถี่วิทยุเป็นสัญญาณความถี่กลางที่ความถี่ 1.45 GHz สายอากาศที่นำเสนอนี้สามารถลดปัญหาสัญญาณออสซิลเลเตอร์ประจำเครื่องที่ส่งออกมาขณะผสมสัญญาณโดยการใช้โครงสร้างวงแหวนแบบไฮบริด ผลการทดสอบแสดงค่าการแยกโดดเดี่ยวระหว่างด้านที่รับสัญญาณความถี่ออสซิลเลเตอร์ประจำเครื่องกับด้านที่รับความถี่วิทยุมีมากกว่า 20 dB ที่ความถี่ 18.298 GHz ค่าการสูญเสียจากการแปลงผันลงแบบไอโซทรอปิกมีค่าน้อยกว่า 15 dB ที่ความถี่ 18.8 GHz ลำดับต่อมาเป็นการทดสอบและสาธิตการทำงานหลายลำคลื่นด้วยสายอากาศผสมสัญญาณหลักการกึ่งแสง 4X1 องค์ประกอบและการทำงานหลายลำคลื่นสามารถกำหนดได้จากระบุมุมของสายอากาศส่งสัญญาณออสซิลเลเตอร์ประจำเครื่องในแต่ละความถี่ซึ่งทั้งหมดทำงานในเวลาเดียวกัน โดยผลการวัดแสดงแบบรูปการแผ่พลังงานสามทิศทางที่วัดได้จากสัญญาณความถี่กลาง ท้ายสุดได้นำเสนอการวัดคุณสมบัติค่าไดอิเล็กตริกของตัวกลางที่มีการสูญเสียโดยใช้วิธีย้อนกลับ ซึ่งวิธีดังกล่าวใช้การวัดที่ตำแหน่งต่างๆ โดยใช้สายอากาศผสมสัญญาณแบบหลักการกึ่งแสง ผลที่ได้แสดงค่าผิดพลาดน้อย

กว่า 11 เปอร์เซ็นต์ซึ่งมีความเป็นไปได้ในการนำไปใช้งานด้านการวัดคุณสมบัติค่าไดอิเล็กตริกของตัวกลางแบบไม่ทำลาย

Thesis Title	A Study on Characteristics of a Quasi-optical Antenna-mixer and Its Applications
Student	Mr.Suwan Janin
Student ID.	47060002
Degree	Doctor of Engineering
Program	Electrical Engineering
Year	2008
Thesis Advisor	Prof.Dr.Monai Krairiksh
Thesis Co-Advisor	Dr.Keattisak Sripimanwat

ABSTRACT

This thesis addresses a principle of quasi-optical antenna-mixer and its applications. Theoretical background of quasi-optical antenna-mixer and beam scanning formulations is analyzed and illustrated for understanding its fundamental. At first, the antenna composed of a quasi-optical hybrid ring antenna-mixer is investigated at K-band. The antenna element consists of back-to-back aperture coupled inverted square patch antenna to couple the RF signal at 18.8GHz to the sigma port of a hybrid ring mixer while the LO signal at 17.5GHz is coupled to the delta port. The HSCH-9101 Schottky diodes are used to transform the RF signal to intermediate signal at 1.45GHz. This antenna mitigates the retransmitted LO signal problem by using hybrid ring structure. The results show the isolation between the LO to RF is better than 20 dB at 18.3GHz, and the isotropic conversion loss of lower sideband is better than 15 dB at 18.8GHz. Next, the 4x1 quasi-optical hybrid ring antenna-mixers are demonstrated and measured. The multibeam operation can be defined by fixing the angle of the LO transmitting antenna at each LO frequency that will be operated at the same time. The results show three IF signals and three radiation patterns. Finally, the dielectric property determination of lossy medium by an inverse technique is implemented in spatial domain by using quasi-optical antenna mixers. The results show the error is less than 11% which is feasibly useful in non-destructive dielectric property determination.

ACKNOWLEDGEMENTS

This thesis could not be completed without the assistance of many persons. I would like to express my appreciation.

First, I am deeply grateful to my advisor, Professor Monai Krairiksh, who has given many research ideas, suggestions and his guidance throughout the course of this research and I would like to thank my co-advisor, Dr.Keattisak Sripimanwat, a leader of the Optical Quantum Communications Laboratory, at the National Electronics and Computer Technology Center, for providing opportunity and support during of this research.

My thanks also go to Associate Professor Sompol Kosulvit and Assistant Professor Chuwong Phongcharoenpanich for their helpful discussions.

I would like to thank Mr.Songmoung Nundrakwang, Department of Control Engineering, Faculty of Engineering, King Mongkut's Institute of Technology Ladkrabang, for whom offered the antenna supporter.

I wish to thank all people in Wireless Communication Laboratory for their kind supports and providing a friendly atmosphere during the work.

I am grateful to the Thailand Graduate Institute of Science and Technology (TGIST), an academic institute of National Science and Technology Development Agency, which provides financial assistance throughout the Ph.D. Program (Grant No. TG-B-11-44-22-717D).

Special thanks go to Ms.Chongthicha Tareejit for her patience, understanding and cheerfulness during a long period of my Ph.D. course.

Finally, I wish to express my gratitude to my parents, Mr.Boonsiong and Mrs.Ruentha Janin for their excessively love, understanding and encouragement throughout my entire life.

Suwan Janin

TABLE OF CONTENTS

TABLE OF CONTENTS (continued)

Page

LIST OF TABLES

LIST OF FIGURES

LIST OF FIGURES (continued)

LIST OF FIGURES (continued)

CHAPTER 1
INTRODUCTION

1.1 Historical notes on quasi-optical antenna-mixers

Wireless communications have been rapidly developed to serve the demand of high speed data communications. With respect to this demand, antennas must be elaborately developed to improve communication capacities. However, the higher frequency causes the higher insertion loss in the radio frequency (RF) circuits particularly in the phase shifters. A quasi-optical antenna-mixer, with the RF signal is transformed by the local oscillator (LO) signal to the intermediate frequency (IF) at the antenna, was proposed to resolve transmission line loss at millimeter wave frequency [1]. It composes of the slot ring resonator loaded by a pair of mixer diodes [2]. Stephan, *et al.* proposed the means of a newly defined quasi-optical mixer parameter called isotropic conversion loss [3]. The millimeter-wave front-end utilized quasi-optical integrated antenna has been proposed in [4]. Planar quasi-optical receivers that compactly integrate a coupled slot antenna with a HEMT or MESFET balanced self-oscillating mixer on the same substrate was developed [5] for applications in microwave and millimeter-wave receiver arrays. The conversion gain was improved by adding the hemispherical lens [6]. The conversion loss can be further improved by using the magic slot-lens radiator [7]. A planar quasi-optical mixer using a folded-slot antenna excited by orthogonal mode was proposed for RF/IF isolation filter [8]. A micromachining technology was used to create a new alternative for submillimeter-wave system [9]. The quasi-optical power combiner is an alternative technique to combine power when the solid state devices can not stand high power as frequency increases.

For power combiner, at millimeter or submillimeter wave combiner, the work in [10] used a quasi-optical open resonator to effectively combine the power output of several solid-state oscillators to a single-frequency. It was shown in [11] that a planar source array containing 25 individual elements or more result in very efficient power transfer of energy from the source arrays. York and Compton [12] proposed the InP Gun resonator of 60GHz with 54% power combine efficiency. The work in [13] demonstrates the power combiner composed of GaAa IMPATT for 100GHz source

and tested by increasing the element of 5x5, 7x7 and 9x9 with obtained corresponding power of 300mW, 630mW and 800mW, respectively. The active planar array of quasi-optical power combiner served by 16 MESFET devices for 10W X-band high power source was proposed in [14]. Wu and Chang discussed an effect of coupling between active circular patch antennas on combined radiation and proposed a novel radiating element with low cross-polarization feature [15]. However, the strong coupling is usefulness for 4×4 power-combining array in multilayer structure as shown in [16]. The application of these two types of connections in the two-dimensional array was discussed. A multilayer (3-D) structure was employed in the circuit design to accommodate the complex layout of the two-dimensional arrays.

A quasi-optical amplifier, is a technique that incoming power is combined as discussed above. When using at high frequency, the high power from solid state devices such as amplifiers can not be obtained. Chi and Rebeiz presented a quasi-optical amplifier suitable for Gaussian-beam applications which composes of horn antenna connected with active devices that provided 10.5dB of gain at 5.92GHz [17]. The researches on quasi-optical amplifiers are reported in [18-20].

For a beam scanning system, the quasi-optical mixer-antenna array has been proposed by Nishimura *et al.* in [21]. The receiving mainbeam of RF signal can be controlled by adjusting LO frequency or changing LO incoming direction. The magnetic loop quasi-optical antenna-mixer in planar array was proposed by Satio *et al.* in [22]. The receiving RF main beam can be scanned similarly in 2D plane.

The knowledge of complex permittivity is important in a great number of applications. Industrial microwave heating requires the precise permittivity determination of the involved dielectric materials. In food industries, accurate measurement of ingredient of the product is very important in manufacturing process. The measuring technique based on cavity perturbation and transmission lines provide accurate results. Free space methods are nondestructive technique that usually suffers from reduced accuracy due to unwanted reflections of the surrounding object and the diffraction from the edges of the sample. Since some objects can not be destructively determined, hence nondestructive determination of unknown dielectric object is important and has been widely developed [23]. Measurement of the reflection spectrum over a wide bandwidth permits one to get rid of spurious solution. This technique provides accurate results by measuring reflected wave from an object, typically layered dielectric sheet with large size comparing to operating wavelength.

Microwave stepped-frequency radar can provide both deep penetration and fine resolution simultaneously for subsurface evaluation [24]. There is only one drawback that it needs wideband measurement which requires expensive measuring instruments. When frequency spectrum is limited, a narrow band measurement is desirable.

In an inverse technique for dielectric property determination applications, the use of quasi-optical antenna-mixer is feasible because the measurement in spatial domain [25] can provide as accurate results as those from the measurement in frequency domain. This technique has a significant advantage that single LO is used, hence synchronization between LO is not necessary as in the conventional multiple superheterodyne receivers. Nevertheless, LO retransmission is a severe problem when it reflects back from the object under determination to the mixer and results in measurement error. Therefore, mitigation of LO retransmission must be carried out.

1.2 Research objectives

In this thesis, the study on a quasi-optical antenna-mixer is proposed. The nature of quasi-optical antenna-mixer is based on receiving the RF and LO signals in front and back sides of the antenna. Therefore, the undesired problem occurs in the mixing operation. The LO retransmitting signal through the back side to the front side perturbs the outside environment that is a serious problem in wireless communication systems. The hybrid ring coupler, embedded in quasi-optical antenna mixer, is presented to alleviate the undesired LO retransmitting signal.

In multiple-beam operation, those techniques in [21], [22] cannot fulfill the requirement that the antenna system should provide multiple-beam instead of single beam operation. These antenna-mixers can scan the mainbeam by controlling the LO's incoming incident angle. However, the work in [21] provides a single beam that cannot fulfill the requirement of the system like Multiple Input Multiple Output (MIMO) system [26]–[27] and angle diversity [28] systems. These systems need an antenna that provides multiple beams simultaneously. The multiple beams antenna with multiple LO transmitting antennae using quasi-optical antenna-mixer is proposed in this thesis.

The details in this research are divided into seven chapters as follow:

Chapter 2 deals with the theory background of quasi-optical antenna-mixer and beam scanning formulation. The analysis and design of antenna element for obtaining high isolation are carried out and tested in chapter 3. A multibeam antenna using quasi-optical hybrid ring mixer antenna array is proposed in chapter 4. Some applications where multibeam antenna is required at high frequency, a quasi-optical antenna mixer array using multiple of LO can be accomplished with different LO frequencies. Multibeam antenna can be accomplished with different intermediate frequencies. The quasi-optical mixer is used to operate as multibeam antenna. The direction of the RF receiving beam is defined by the direction of LO transmitting antenna. In order to produce a multibeam antenna without a complicated feeding system, this thesis proposes the use of quasi-optical antenna-mixers. Multiple LO transmitters at different frequencies are used to provide multibeam at different IF frequencies. By taking element patterns into account, accurate beam directions can be accomplished. This kind of multibeam antenna is useful for modern wireless communications. The effect of non-uniform plane wave on radiation pattern of a quasi-optical antenna-mixer array is discussed and the accurate design can be achieved. It is presented in chapter 5. To accomplish the simple measuring system with accurate result, chapter 6 demonstrates an implementation of an inverse measurement system using quasi-optical antenna mixers for measuring reflected wave in spatial domain. Comparison of simulation results in frequency and spatial domains will be illustrated. Causes of error will be discussed that show the potential of the system in practical use. The calibration process is proposed and measurement results by this technique are compared with the ones from the dielectric probe. Chapter 7 details the overall conclusions and discussions of the results obtained form this study and recommendation for the further research.

CHAPTER 2
FUNDAMENTAL OF A QUASI-OPTICAL ANTENNA - MIXER

2.1 Introduction

This chapter describes a foundation of quasi-optical antenna-mixer and beam scanning technique by using quasi-optical antenna-mixer array. Since high insertion loss in the circuits particularly in the phase shifters is a serious problem at the high frequency such as in millimeter wave band, a quasi-optical antenna mixer array was proposed to overcome losses from the used transmission lines [1]. It can scan the mainbeam without using phase shifters [21]-[22]. These antennae consist of a back-to-back rectangular-patch antenna fed by a CPW (Coplanar Waveguide) and Schottky-barrier diode. The mainbeam to receive Radio Frequency (RF) incoming signal direction can be scanned by moving the direction of the Local Oscillator (LO) transmitting antenna and changing the LO frequency.

2.2 A quasi-optical antenna-mixer operation

In the conventional receiver, RF and LO signals are fed through transmission lines to a mixer as shown in Fig. 2.1(a). As frequency increases, insertion loss of the transmission line typically increases depending on its transmission line length. Due to this problem, the quasi-optical antenna-mixer was proposed to reduce the losses. The concept of quasi-optical antenna mixer, where RF is transformed to IF (Intermediate Frequency) signal at the antenna is shown in Fig. 2.1(b). The RF receiving antenna and the LO receiving antenna are installed in a back-to-back manner. This technique occupies an important position in the practical use of millimeter wave systems.

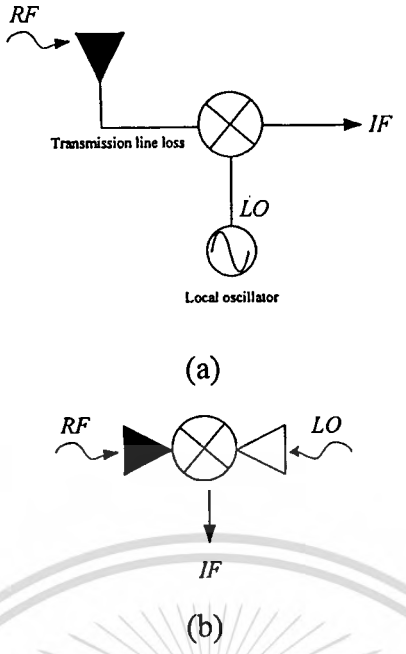

Fig. 2.1 Receiving systems (a) Conventional heterodyne receiver (b) Quasi-optical antenna-mixer

2.2.1 Mixer operation

In radio communication, the IF signal is shifted to the RF frequency that is suitable for electromagnetic propagation at the transmitter. The receiving frequency is shifted into the baseband frequency to obtain the information. The frequency shifting is called mixing by using nonlinear devices.

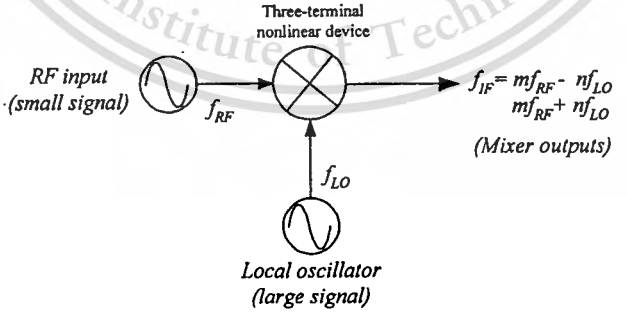

Fig. 2.2 Mixer model

A mixer is a three-port device as shown in Fig. 2.2, which consists of an input RF signal port, an output IF signal port and a local oscillator (LO) port. The LO port is

used to drive the mixer, and the LO power is normally higher than the RF signal. This driving action sometimes is called switching or modulation.

In case of RF and LO signals without harmonic and noise, the mixing products or outputs of the mixer are illustrated in Fig. 2.3. These outputs consist of upper (f_{RF} + f_{LO}) and lower sideband (f_{RF} - f_{LO}) products.

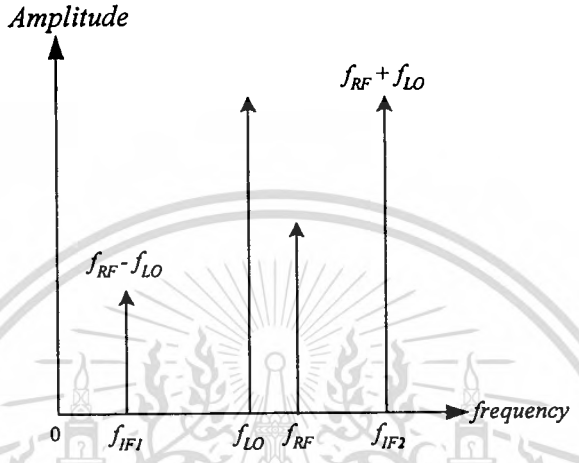

Fig. 2.3 Output spectrum of mixing product

Mixing is achieved by injecting two signals to a nonlinear device. The output of mixer can be expressed as

$$I = K(V + v_1 + v_2)^n \tag{2.1}$$

where n is an exponential constant, V is an offset or biasing voltage that is applied to mixer diode, $v_1 = V_1 \sin(\omega_1 t)$ is an RF signal, and $v_2 = V_2 \sin(\omega_2 t)$ is the LO signal. When n =2, (2.1) becomes

$$I = K\left[V + V_1 \sin(\omega_1 t) + V_2 \sin(\omega_2 t)\right]^2 \tag{2.2}$$

$$I = K\Big[V^2 + V_1^2 \sin^2(\omega_1 t) + V_2^2 \sin^2(\omega_2 t) + 2VV_1 \sin(\omega_1 t) + 2VV_2 \sin(\omega_2 t) + 2V_1V_2 \sin(\omega_2 t)\sin(\omega_1 t)\Big] \tag{2.3}$$

The output signal in (2.3) shows that it comprises of many terms of signals. We emphasize on the output term that generates the IF signal which consists of V_1 and V_2. Therefore, (2.3) reduces to

$$I_{IF} = 2KV_1V_2 \sin(\omega_1 t)\sin(\omega_2 t) \tag{2.4}$$

$$I_{IF} = KV_1V_2\left\{\cos\left[(\omega_2 - \omega_1)t\right] - \cos\left[(\omega_2 + \omega_1)t\right]\right\} \tag{2.5}$$

Equation (2.5) shows the upper and lower bands of the IF signals which one of interest will be selected by using an IF filter.

2.2.2 180^0 Hybrid ring or rat-race ring coupler

A hybrid ring coupler is a basic transmission line circuit for balance diode mixer. It is a four port device, and all ports are matched with standard 50Ω impedance. The structure of a hybrid ring or rat-race ring coupler is illustrated in Fig. 2.4.

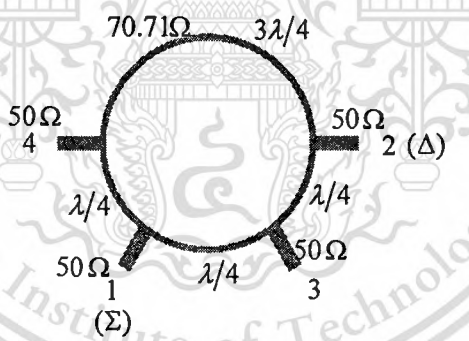

Fig. 2.4 180^0 Hybrid ring or rat-race ring coupler

If the RF power is inserted to the port 1(Σ), it is equally spitted to port 3 and 4 with power of -3dB lower than the input at port 1. Port 2(Δ) is used as the isolated port that is 180^0 of phase difference comparing with the port 1 while the LO incoming signal arrives at port 2. The electrical length from port 1 to port 2 in the counter clockwise direction is $\lambda/2$ and it is λ in the clockwise direction. It means that the corresponding phase differences 180° and 360°, respectively. Consequently, the

hybrid ring can isolate the LO incoming signal to the RF receiving port. The fundamental of hybrid ring coupler can be described by using the S-matrix as

$$S = \frac{1}{\sqrt{2}} \begin{bmatrix} 0 & S_{12} & S_{13} & S_{14} \\ S_{21} & 0 & S_{23} & S_{24} \\ S_{31} & S_{32} & 0 & S_{34} \\ S_{41} & S_{42} & S_{43} & 0 \end{bmatrix} \tag{2.6}$$

and

$$S = \frac{1}{\sqrt{2}} \begin{bmatrix} 0 & 0 & 1 & 1 \\ 0 & 0 & 1 & -1 \\ 1 & 1 & 0 & 0 \\ 1 & -1 & 0 & 0 \end{bmatrix} . \tag{2.7}$$

To consider isolation by using S-matrix, the hybrid ring coupler can be chosen in two cases. One is to select port 1 and port 2 because $S_{21} = S_{12} = 0$. The other is to select port 3 and port 4 with $S_{43} = S_{34} = 0$. These mean that no power is coupled through these ports. This thesis uses the hybrid ring coupler to improve RF/LO isolation of the quasi-optical antenna-mixer and an analysis and design will be shown in Chapter 3.

2.2.3 Isotropic Conversion Loss of quasi-optical antenna-mixer

Since a quasi-optical antenna-mixer combines the functions of antenna and mixer, the conventional definitions of antenna gain and mixer conversion loss cannot be used to determine circuit performances. To characterize the efficiency of the receiver, the isotropic conversion loss L_{iso}, is defined as

$$L_{iso} = 10\log\left(\frac{P_{IF}}{P_{iso}}\right) dB \tag{2.8}$$

where P_{IF} is the down-converted IF power signal. P_{ISO} is the RF power that is obtained by receiving RF signal when the antenna gain is taken into account. It is compared with the same antenna under the same measurement conditions.

2.3 Fundamental of a beam scanning system by using quasi-optical antenna-mixer array

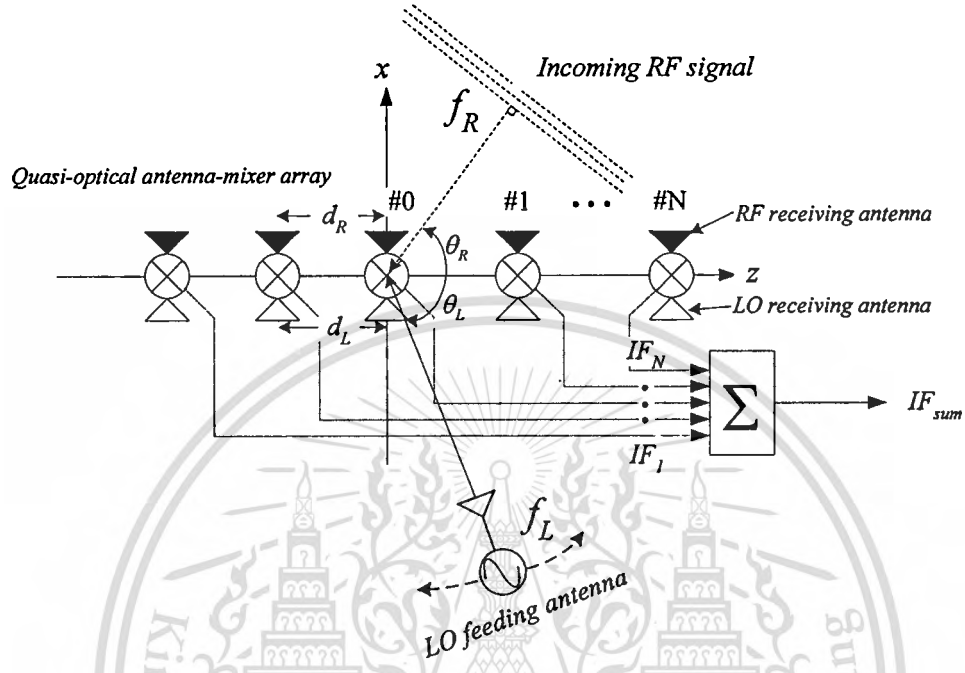

Fig. 2.5 Diagram of a quasi-optical antenna-mixer array

The diagram of a quasi-optical antenna-mixer array is shown in Fig. 2.5. The quasi-optical antenna-mixer elements are placed on the *z*-axis and the RF signal incidents on the upper side of the quasi-optical antenna-mixers. The LO transmitting antenna for transmitting LO signal is placed on the lower side in the far-field range. The received RF signal is transformed to IF signal at each array element and are combined at a power combiner. The LO signal plane wave, radiated by an LO transmitting antenna, in the direction θ_L is used to control the main beam of the antenna to receive RF incoming signal at the direction θ_R. The amplitude of RF signal of the n^{th} element is

$$E_{R,n} = S_{R,n} \times D_{R,n} \tag{2.9}$$

where $S_{R,n}$ is electric field intensity of the signal arriving at the n^{th} element and $D_{R,n}$ is the element pattern of the n^{th} element. In the same manner, the LO amplitude on the n^{th} element is expressed as

$$E_{L,n} = S_{L,n} \times D_{L,n} \tag{2.10}$$

where $S_{L,n}$ is electric field intensity of the LO signal arriving at the n^{th} element and $D_{L,n}$ is the element pattern of the LO receiving antenna. The phase differences between two elements for the RF and LO signals, φ_R and φ_L, are defined as

$$\varphi_R = k_R \cdot d_R \cdot \cos\theta_R \tag{2.11}$$

$$\varphi_L = k_L \cdot d_L \cdot \cos\theta_L \tag{2.12}$$

where k_R and k_L are wave numbers for the RF and LO signals, respectively. d_R and d_L are element separations between RF and LO receiving elements, respectively. The RF signal is transformed by a quasi-optical antenna-mixer into an IF signal. The IF output in the n^{th} element is

$$I_n = E_{R,n} \cdot \cos(\omega_R t - n\varphi_R) \otimes E_{L,n} \cdot \cos(\omega_L t - n\varphi_L)$$

$$= \frac{1}{2} K_n E_{R,n} E_{L,n} \times \left[\cos\{(\omega_R - \omega_L)t - n(\varphi_R - \varphi_L) + \beta_{n-}\}\right.$$
$$\left. + \cos\{(\omega_R + \omega_L)t - n(\varphi_R - \varphi_L) + \beta_{n+}\}\right]$$

$$= A_n\left[\cos(\Omega_- t - n\Psi_- + \beta_{n-}) + \cos(\Omega_+ t - n\Psi_+ + \beta_{n+})\right] \tag{2.13}$$

where ω_R and ω_L are angular frequencies of the RF and LO signals, respectively. K_n is the conversion gain of the mixer, and

$$A_n = \frac{1}{2} K_n E_{R,n} E_{L,n} \tag{2.14}$$

$$\Omega_- = \omega_R - \omega_L \tag{2.15}$$

$$\Omega_+ = \omega_R + \omega_L \tag{2.16}$$

$$\psi_- = \varphi_R - \varphi_L \tag{2.17}$$

$$\psi_+ = \varphi_R + \varphi_L \tag{2.18}$$

β_{n-} and β_{n-} are the phase differences from the transmission line. In general, the $\otimes$ symbol represents the mixing operation. It is defined as the operator to multiply the product of both sides of the symbol by the conversion gain. These IF outputs are combined by using the Wilkinson power combiner [29]. Therefore, the combined IF signal is obtained as

$$I_{sum} = c \cdot \sum_{n=1}^{N-1} I_n \tag{2.19}$$

where c is a constant depended on the number of antenna-mixer elements. For simplicity, we assume that the amplitude of conversion gain of RF and LO incoming signals of each antenna-mixer are uniform. Moreover, the phase references (ψ_- and ψ_+) are moved to the phase of a linear array factor [30]. Equation (2.19) becomes

$$IF_{sum} = IF_{dc} \cos(\Omega_- t) + IF_{uc} \cos(\Omega_+ t) . \tag{2.20}$$

Therefore, the radiation patterns of linear array factor of IF signal can be separated into two cases. One is the radiation for down conversion. The other is for up

conversion, and the maim beam of each case are in opposite directions. These array factors are given by

$$AF_{down} = \sum_{i=1}^{n} e^{j(n-1)(k_R d_R \cos\theta_R - k_L d_L \cos\theta_L)} \tag{2.21}$$

and

$$AF_{up} = \sum_{i=1}^{n} e^{j(n-1)(k_R d_R \cos\theta_R + k_L d_L \cos\theta_L)} . \tag{2.22}$$

It should be noted that (2.21) and (2.22) are used when the element pattern of quasi-optical antenna-mixer element is an isotropic radiation pattern. The maximum mainbeam direction of the antenna can be achieved by setting the term of the phase references (ψ_- and ψ_+) equal to 0^o. For down conversion, the maximum mainbeam of incoming RF signal can be derived as follow;

$$\psi_- = 0$$

$$k_R d_R \cos\theta_R - k_L d_L \cos\theta_L = 0$$

$$k_R d_R \cos\theta_R = k_L d_L \cos\theta_L$$

$$\cos\theta_R = \frac{k_L d_L \cos\theta_L}{k_R d_R} \tag{2.23}$$

where $k_L = \frac{2\pi}{\lambda_L} = \frac{2\pi f_L}{c}$ and $k_R = \frac{2\pi}{\lambda_R} = \frac{2\pi f_R}{c}$. Therefore, (2.23) is

$$\theta_{R,downconv.}\Big|_{\max} = \cos^{-1}\left(\frac{f_L d_L \cos\theta_L}{f_R d_R}\right). \tag{2.24}$$

Similarly, the maximum of RF receiving direction is written as

$$\psi_+ = 0$$

$$k_R d_R \cos\theta_R + k_L d_L \cos\theta_L = 0$$

$$k_R d_R \cos\theta_R = -k_L d_L \cos\theta_L$$

$$\cos\theta_R = -\frac{k_L d_L \cos\theta_L}{k_R d_R} \tag{2.25}$$

where $k_L = \frac{2\pi}{\lambda_L} = \frac{2\pi f_L}{c}$ and $k_R = \frac{2\pi}{\lambda_R} = \frac{2\pi f_R}{c}$. Therefore, (2.25) is

$$\theta_{R,upconv.}\Big|_{\max} = \cos^{-1}\left(\frac{f_L d_L \cos\theta_L}{f_R d_R}\right). \tag{2.26}$$

Equations (2.24) and (2.26) are used to predict the maximum mainbeam for receiving RF signal. Fig. 2.6 shows the relation of down conversion receiving RF signal direction (θ_R) depending on the LO transmitting antenna direction (θ_L) when the frequency ratio (f_L/f_R) is varied from 0.7 to 1.3 with step of 0.1. The results show that the receiving RF signal direction (θ_R) is sensitive with the LO transmitting antenna direction (θ_L). In cases of (f_L/f_R) are 0.7, 0.8 and 0.9, which mean that the LO frequencies are less than RF frequency, the scan limit of RF receiving directions are 45.6 to 134.4, 36.9 to 143.1, and 25.8 to 154.2 degrees, respectively. However, in case of (f_L/f_R) are 1.1, 1.2 and 1.3, the scan limit of RF receiving directions are between 0 to 180 degrees can be accomplished by moving the LO transmitting antenna direction (θ_L) form 22 to 156, 32 to 148, and 38 to 142 degrees, respectively. These results are important for a quasi-optical beam scanning performance. For up conversion, Fig. 2.7 shows the relation of up conversion of receiving RF signal direction (θ_R) depending

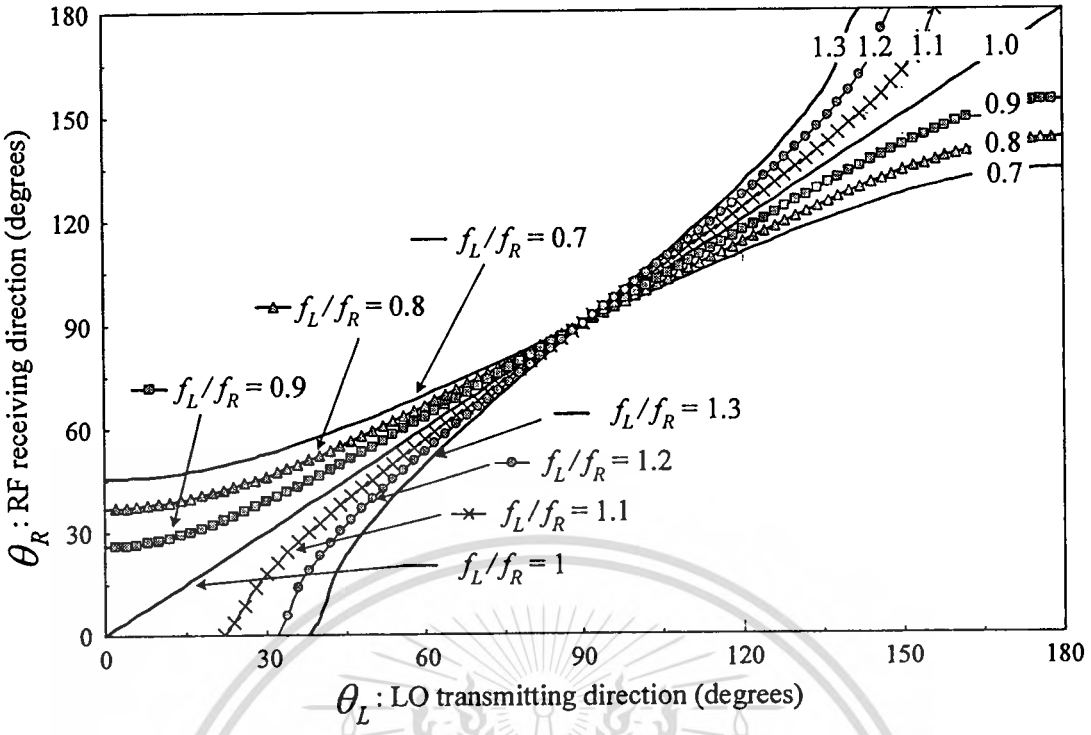

Fig. 2.6 Relation of θ_R depended θ_L with varied frequency ratio (f_L/f_R) when d_R=d_L for down conversion

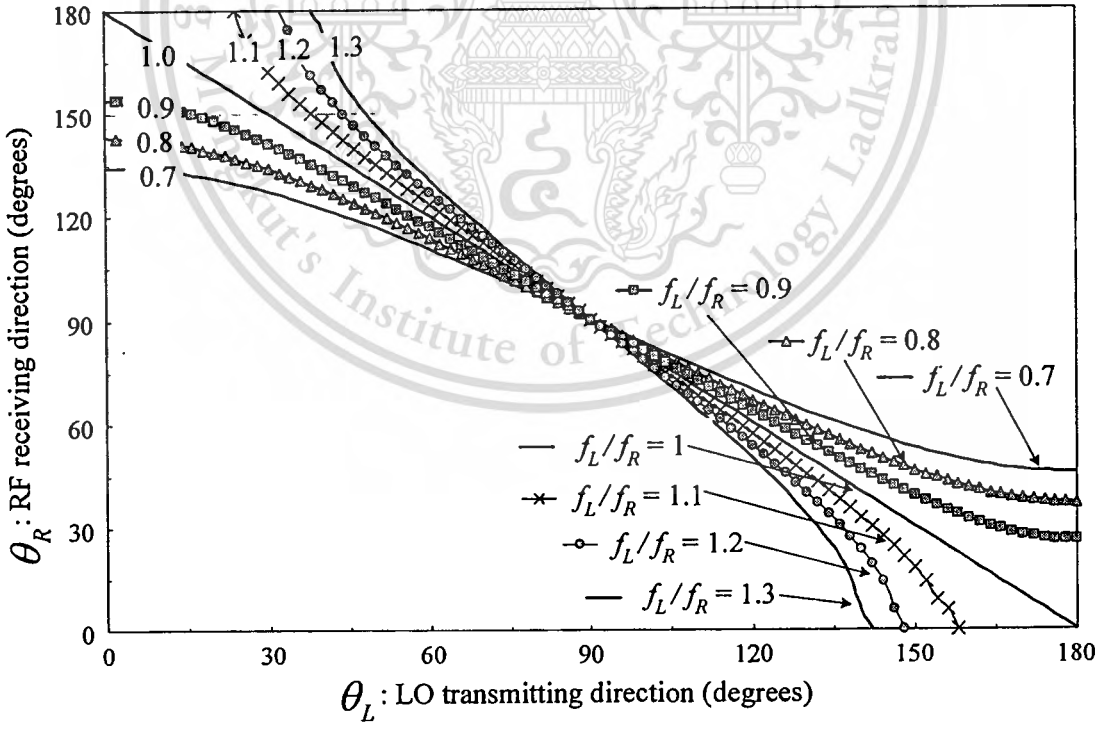

Fig. 2.7 Relation of θ_R depended θ_L with varied frequency ratio (f_L/f_R) when d_R=d_L for up conversion

on the LO transmitting antenna direction (θ_L) when the frequency ratio (f_L/f_R) is varied from 0.7 to 1.3 with step of 0.1. The results show that the receiving RF signal direction (θ_R) is sensitive with the LO transmitting antenna direction (θ_L). In cases of (f_L/f_R) are 0.7, 0.8 and 0.9, which mean that the LO frequencies are less than RF frequency, the limit of RF scan directions are 134.4 to 45.6, 143.1 to 36.9, and 154.2 to 25.8 degrees, respectively. However, in case of (f_L/f_R) are 1.1, 1.2 and 1.3, the limit of RF scan directions is 0 to 180 degrees of all directions by moving the LO transmitting antenna direction (θ_L) form 24 to 158, 32 to 148, and 38 to 142 degrees, respectively. By comparing Fig. 2.6 and 2.7, those results can confirm that the directions for receiving RF signal in the up and down conversion are in opposite directions. Furthermore, the scanning mainbeam capabilities are critically limited with the frequency ratio. These results can be taken into account for performance consideration of a quasi-optical beam scanning application.

To study the effect of ratio of distances between antennas (d_R/d_L) in case of up and down conversion, Fig. 2.8 and 2.9 illustrate the relation of θ_R depended θ_L with varied distance between RF and LO receiving antenna ratio (d_R/d_L) when f_R=f_L for down and up conversion, respectively.

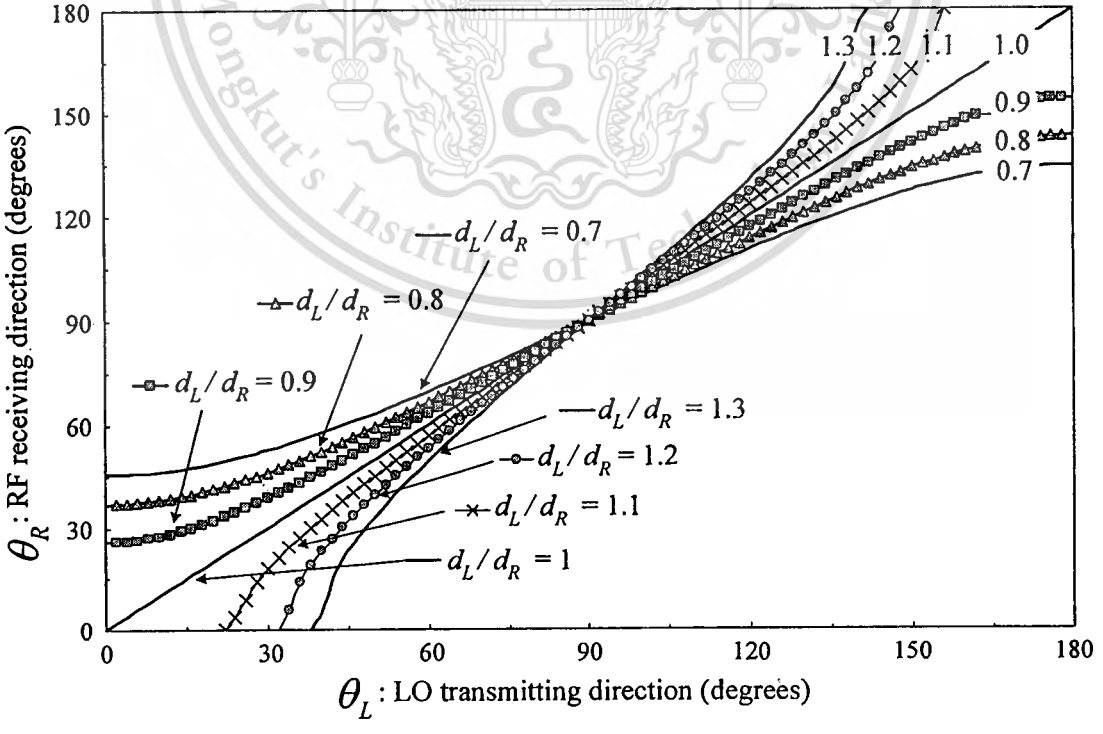

Fig. 2.8 Relation of θ_R depended θ_L with varied distance between RF and LO receiving antenna ratio (d_R/d_L) when the f_R=f_L for down conversion

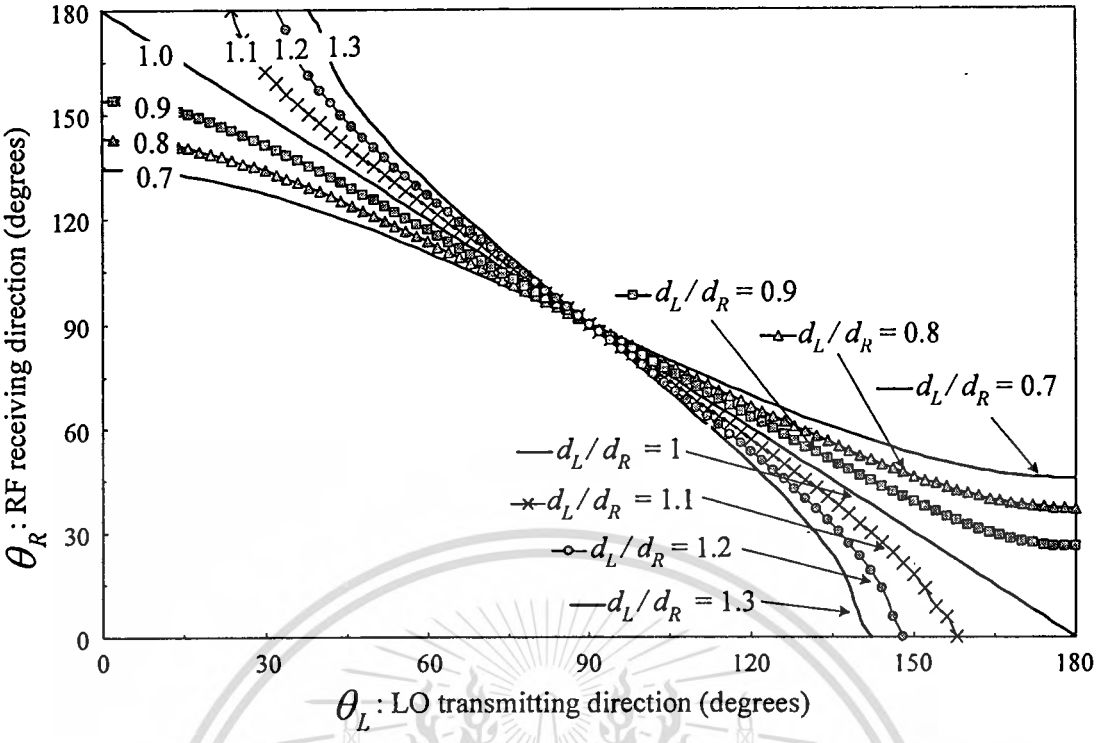

Fig. 2.9 Relation of θ_R depended θ_L with varied distance between RF and LO receiving antenna ratio (d_R/d_L) when the f_R=f_L for up conversion

Fig. 2.8 and 2.9 show that the receiving RF signal direction (θ_R) is sensitive with the LO transmitting antenna direction (θ_L), and the accurate case is that when the distance between RF and LO receiving antenna is the same.

2.4 Beam scanning operation

To demonstrate beam scanning system by quasi-optical antenna-mixer array, we assume that this array composes of a four-element quasi-optical antenna mixer system (N=4), and the distance between element, with d_R=d_L, is 0.5λ. The array is assumed to be linear array of isotropic elements. The combined IF outputs are calculated as a function of θ_R when the frequency ratio (f_L/f_R) are 0.7, 0.8 and 0.9, and the LO transmitting antenna direction (θ_L) are fixed at 45 degrees. In addition, the combined IF radiation patterns are corresponding to the components of down and up conversion. Fig. 2.10(a) shows the down converted main beam of IF radiation pattern can be scanned from 60, 55 and 50 degrees when the frequency ratio (f_L/f_R) are adjusted from 0.7, 0.8 and 0.9, respectively. On the other hand in up conversion, the main beam is in opposite direction of 120, 125 and 130 degrees. These results clearly show that the

change in mixing operation changes the mainbeam in opposite direction. For the fixed ratio of frequency (f_L/f_R = 0.9) and changing θ_L, Fig. 2.11 shows relation of IF

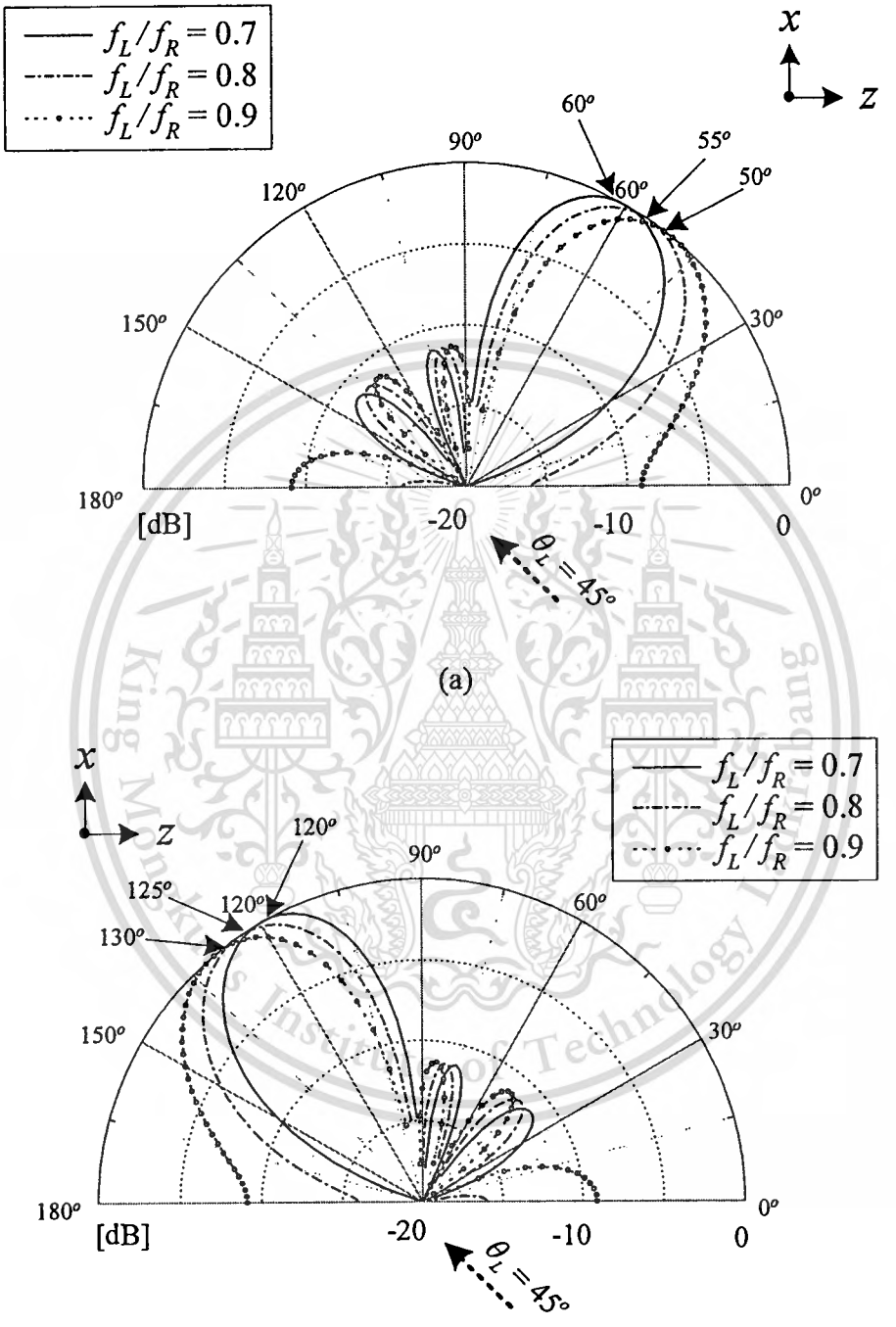

Fig. 2.10 IF radiation pattern when θ_L are fixed at 45 degrees and frequency ratio (f_L/f_R) are 0.7, 0.8 and 0.9 (a) down conversion (b) up conversion

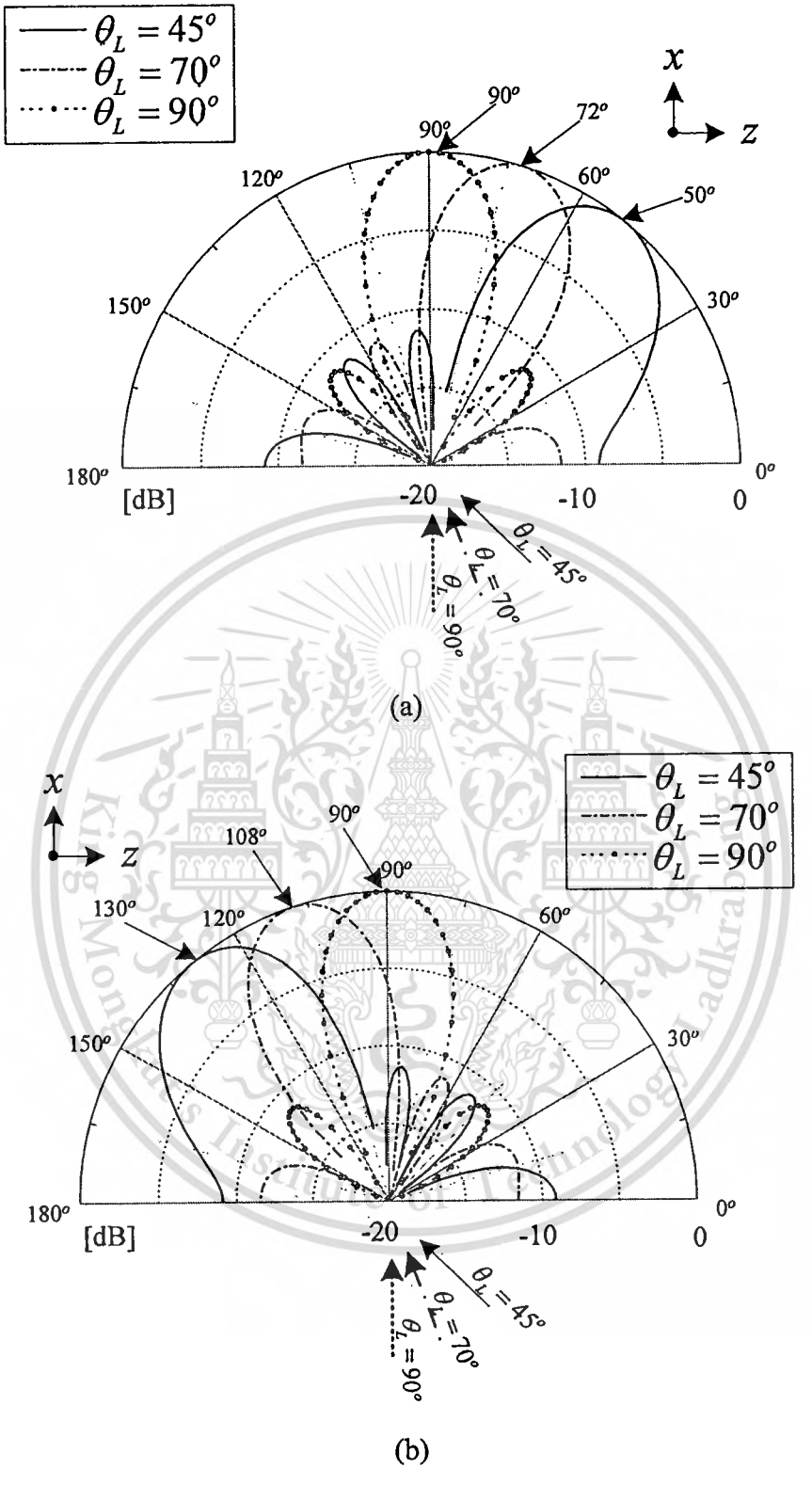

Fig. 2.11 IF radiation pattern when ratio of frequency ($f_I/f_R = 0.9$) and changing the LO transmitting antenna to 45, 70 and 90 degrees (a) down conversion (b) up conversion

radiation pattern when changing the LO transmitting antenna to 45, 70 and 90 degrees, respectively. The calculated results show the mainbeam of IF can be controlled by moving the LO transmitting antenna. Moreover, the mainbeam direction of down conversion is opposite to the up conversion case.

2.5 Conclusion

The fundamental of quasi-optical antenna-mixer and the theoretical background for beam scanning system using this antenna are described and analyzed in this chapter. This antenna is proposed to solve the problem of losses in transmission line. For beam scanning system using quasi-optical antenna-mixer array, the IF receiving main beam direction can be controlled by two means. One is changing the LO transmitting frequency. The other is moving LO transmitting direction. The calculated results show that the receiving IF signal direction (θ_R) is sensitive to the LO transmitting antenna direction (θ_L), and the scanning mainbeam capabilities are critically limited by the frequency ratio. The accurate mainbeam prediction is obtained when the distance between RF and LO receiving antenna ratio (d_R/d_L) is the same.

CHAPTER 3
A HYBRID RING COUPLER QUASI-OPTICAL ANTENNA-MIXER

3.1 Introduction

This chapter describes an analysis and a design of a hybrid ring coupler quasi-optical antenna-mixer for mitigating local oscillator retransmission. The antenna element consists of back-to-back aperture coupled inverted square patch antenna to couple the RF signal at 18.8GHz to the sigma port of a hybrid ring mixer while the LO signal at 17.5GHz is coupled to the delta port. The HSCH-9101 Schottky diodes are used to transform the RF signal to the intermediate frequency signal at 1.3GHz. The results show that the RF/LO isolation is better than 29dB at 18.19GHz, and the isotropic conversion loss of the down converted signal is better than 16dB at 19.25GHz.

3.2 Principle of a hybrid ring coupler quasi-optical antenna-mixer

The hybrid ring quasi-optical antenna-mixer using a hybrid ring coupler to mitigate LO retransmission is shown in Fig. 3.1. Fig. 3.1(a) shows the cross-section of a six-layer antenna element, which consists of an aperture-coupled inverted square patch antenna for receiving RF and LO signals at the top and the bottom layers. The middle layer of the antenna, with mixer diodes, is shown in Fig. 3.1(b). To demonstrate the design at K-band, the aperture-coupled inverted square patch antenna is designed to receive RF and LO signals at 18.8GHz and 17.5GHz, respectively. A hybrid ring mixer is equipped with an impedance stepped low pass filter (LPF). The radius R is designed to obtain high isolation in the LO-to-RF receiving antennas. The strip-foam-slot inverted patch [31] as shown in Fig. 3.1(c), which has the broadband characteristic, low cross-polarization level, integrated radome and low-cost, is used. The inverted square patch antenna at the top layer, with the width l_p, is etched on the patch substrate by using RO3003 PTFE material with height h_1 = 0.762mm and dielectric constant ε_{r1} = 3.

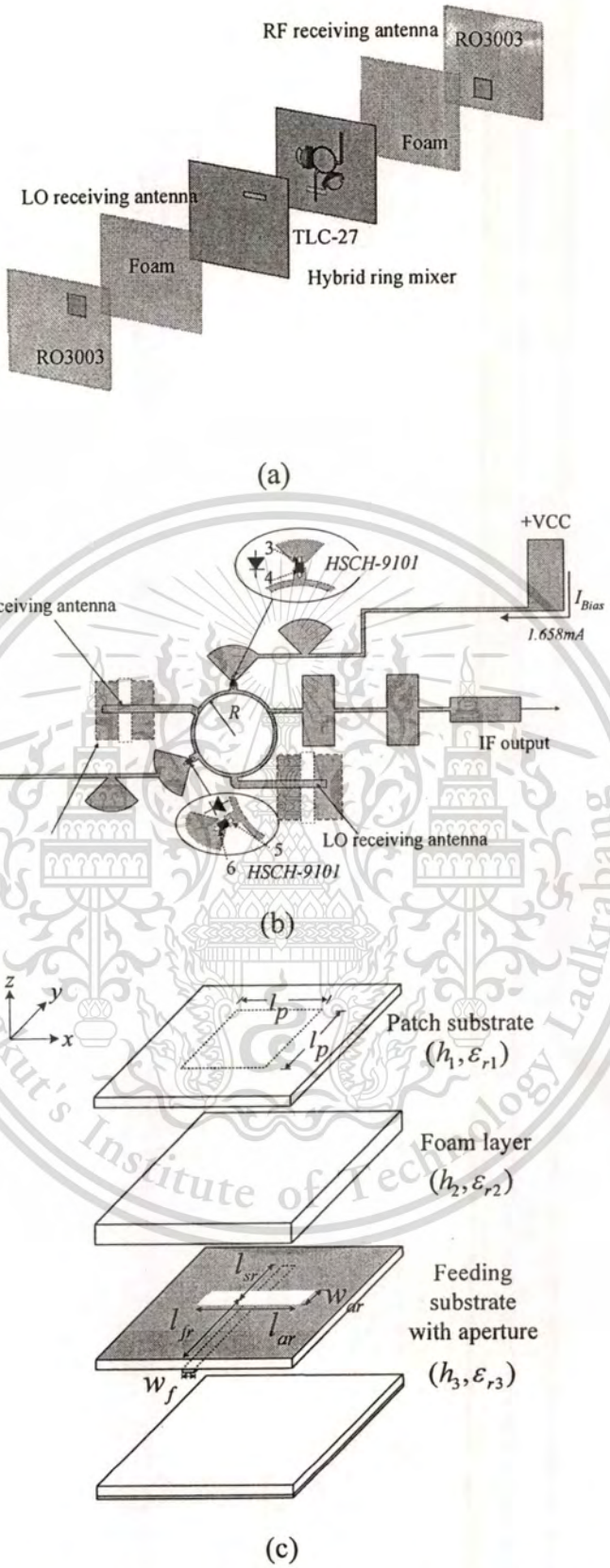

Fig. 3.1 Configuration of the hybrid ring coupler quasi-optical antenna-mixer (a) Six-layer view (b) Layout of hybrid ring with mixer diodes (c) Strip-foam-slot inverted patch

The foam layer with thickness h_2 = 0.5mm and dielectric constant ε_{r2} = 1.07 is inserted between the inverted square patch antenna and the feeding substrate to prevent surface propagation and enhance the impedance bandwidth. The feeding substrate using TLC-27 material is copper cladding on both sides with height h_3 = 0.37mm and dielectric constant ε_{r3} = 2.75. The upper side is a ground plane and a wide aperture is used to increase impedance bandwidth. The lower side is a feeding stripline etched with width w_{ar} and length l_{ar}.

The open radial stub with low impedance line and wide bandwidth is used for creating RF shorted circuit as seen in Fig. 3.1(b). The HSCH-9101 GaAs Beam Lead Schottky Barrier Diodes are mounted between the arm of the ring and the radial stub. The radial stubs with 1.86mm in length and angle of 90^o provide the virtual ground without via hole to ground. The LPF with cutoff frequency at 2GHz is used to capture IF signals and to isolate from the hybrid ring structure.

3.3 Analysis

The important characteristic is the isolation of the LO signal to the RF port. It should be sufficiently high so that LO signal will not be retransmitted. The commercial ADS2001^{TM} [32] based on transmission line model is used to analyze the proposed hybrid ring antenna-mixer. The model is also shown in Fig. 3.1(b). It consists of an 180^o hybrid ring (rat-race) coupler, the mixing diodes (using HSCH9101) and a stepped impedance LPF. It is assumed in the analysis that the mixer diodes are perfectly matched with 50Ω. The TLC-27 substrate, with 0.37mm height, 2.75 dielectric constants and 0.0025 dielectric loss factors, is used to construct the hybrid ring coupler. The width of the 50Ω and 70.71Ω strip-lines are 0.44mm and 0.21mm, respectively. The important parameter of the hybrid ring is a ring radius (R). It is initially designed to be 2.47mm and the circumference is 15.51mm or $1.5\lambda_g$ [29] where λ_g = 10.34mm, is a guided wavelength on the used substrate. The isolation has the maximum value at 17.47GHz, which is slightly shifted from the desired frequency of 17.5GHz. The effect of R on the hybrid ring coupler is studied and shown in Fig. 3.2. It is obvious that the RF/LO isolation ($-10\log\left|P_{LO\ at\ RF\ port} / P_{LO\ at\ LO\ port}\right|$dB) strongly depends on R, and the maximum isolation is obtained when R is 2.465mm.

Both RF and LO receiving antennas must be matched to provide less conversion loss of the antenna-mixer. It is analyzed by using the CST2006^{TM} commercial software [33]. The parameters of the antenna are l_p, l_{ar}, l_{sr}, w_{ar} and h_2. By varying these parameters and plotting resonant frequency between 16-22GHz and impedance bandwidth in the range of 2-23%, the results are shown in Fig. 3.3. The resonant frequency is mainly sensitive to the inverted square patch antenna length (l_p) and the coupling aperture length (l_{ar}). The l_{ar} must be longer than l_p to provide multi resonant frequency. The simulated results are shown in Fig. 3.3(a). The resonant frequency decreases with increasing l_{ar}, l_p and w_{ar} and increases with increasing l_{sr} and h_2. The impedance bandwidth is shown in Fig. 3.3(b). It was found that the impedance bandwidth decreases when l_p increases, and increases when w_{ar}, h_2 and l_{sr} increase.

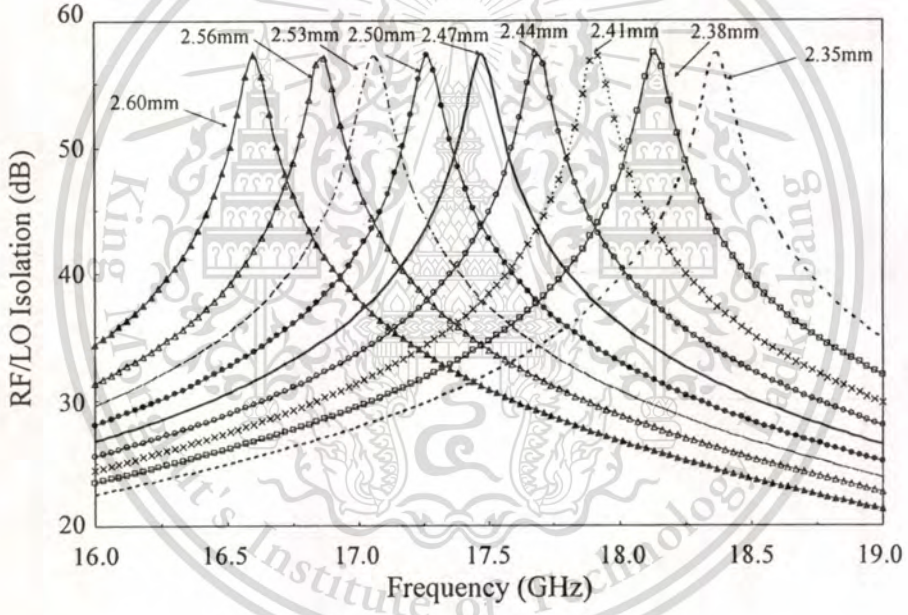

Fig. 3.2 RF/LO Isolation versus frequency for different hybrid ring radii

The graphs in Figs. 3.3(a) and 3.3(b) can be used for designing the RF and LO receiving antennas. With specified bandwidth as shown in Fig. 3.3(b), the appropriate parameters can be selected. Then, the final design parameters are obtained from the resonant frequency in Fig. 3.3(a). For illustration, the bandwidth is specified to be 20% and the resonant frequency is 18.8GHz. The RF receiving antenna has the dimensions as shown in Table 3.1. The simulated return losses of the RF receiving antenna, with parameters in Table 3.1 compared in case of l_{ar} is shorter than l_p, are

shown in Fig. 3.4 which shows that the lower and upper resonant frequencies depend on l_p and l_{ar}, respectively. Fig. 3.4(a) shows that the return loss versus frequency of an RF receiving antenna has narrow frequency response when $l_p > l_{ar}$. On the other hand, the wideband response is obtained when $l_p < l_{ar}$. The impedance bandwidth (-10dB return loss) is 20.8%.

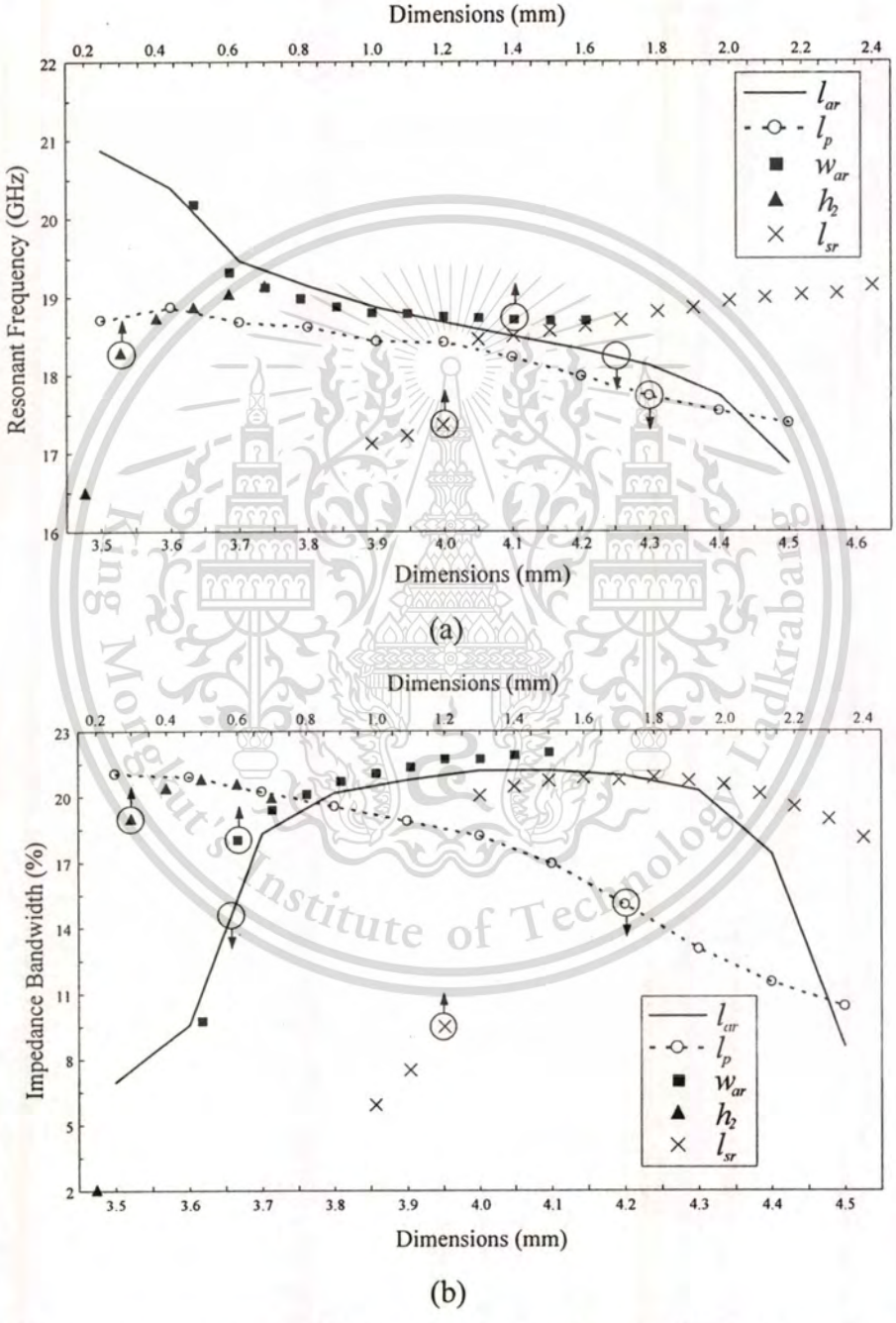

Fig. 3.3 Resonant frequency and impedance bandwidth for different parameters (a) Resonant frequency (b) Impedance bandwidth

Table 3.1 Dimensions of RF receiving antenna (at 18.8GHz)

Parameters	l_p	l_{ar}	w_{ar}	l_{sr}	h_2
Dimensions (mm)	3.60	3.90	0.90	1.80	0.50
Dimensions (λ in each ε_r)	$0.39\lambda_{d\varepsilon r1}$	$0.40\lambda_{d\varepsilon r3}$	$0.09\lambda_{d\varepsilon r3}$	$0.19_{d\varepsilon r3}$	$0.03\lambda_{d\varepsilon r2}$

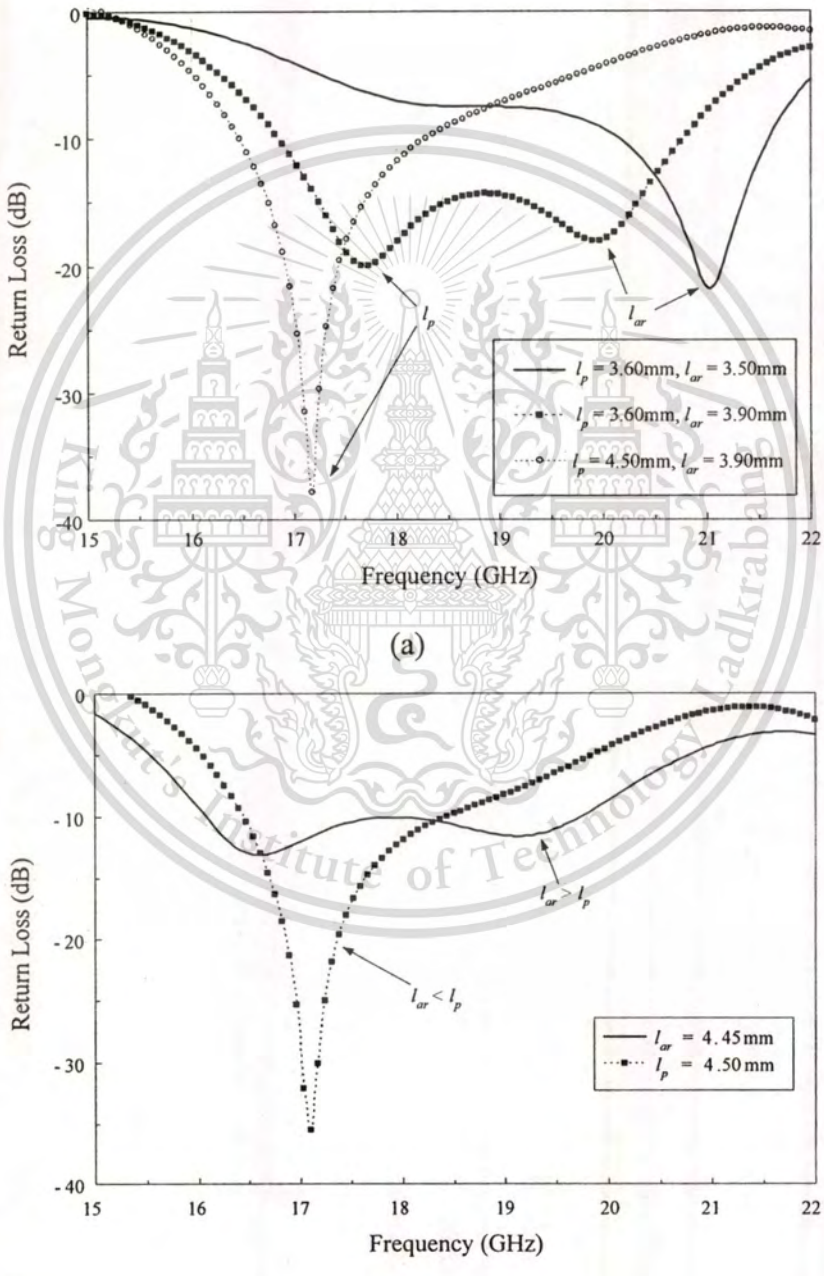

Fig. 3.4 Return loss versus frequency of receiving antennas (a) RF receiving antenna (b) LO receiving antenna

Fig. 3.3(a) and 3.3(b) are also used to design the LO receiving antenna by increasing l_{ar} to 4.45mm or increasing l_p to 4.5mm for decreasing the resonant frequency. The simulated return loss of the LO receiving antenna, with parameters in Table 3.2, is shown in Fig. 3.4(b). The impedance bandwidths are 20% ($l_{ar} > l_p$) and 11.23% ($l_p > l_{ar}$), respectively. It can be confirmed that the impedance bandwidths are enhanced by using l_{ar} longer than l_p.

Table 3.2 Dimensions of LO receiving antenna (at 17.5GHz)

Parameters	l_p	l_{ar}	w_{ar}	l_{sr}	h_2
Dimensions (mm)	3.60	4.45	0.90	1.80	0.50
Dimensions (λ in each ε_r)	$0.36\lambda_{d\varepsilon r1}$	$0.43\lambda_{d\varepsilon r3}$	$0.09_{d\varepsilon r3}$	$0.17\lambda_{d\varepsilon r3}$	$0.03\lambda_{d\varepsilon r2}$

3.4 RF/LO isolation

Since the conventional quasi-optical antenna-mixer in [21] and [22] used a coplanar waveguide fed patch antenna and a magnetic loop antenna, respectively, the high isolation quasi-optical antenna-mixer can not be achieved.

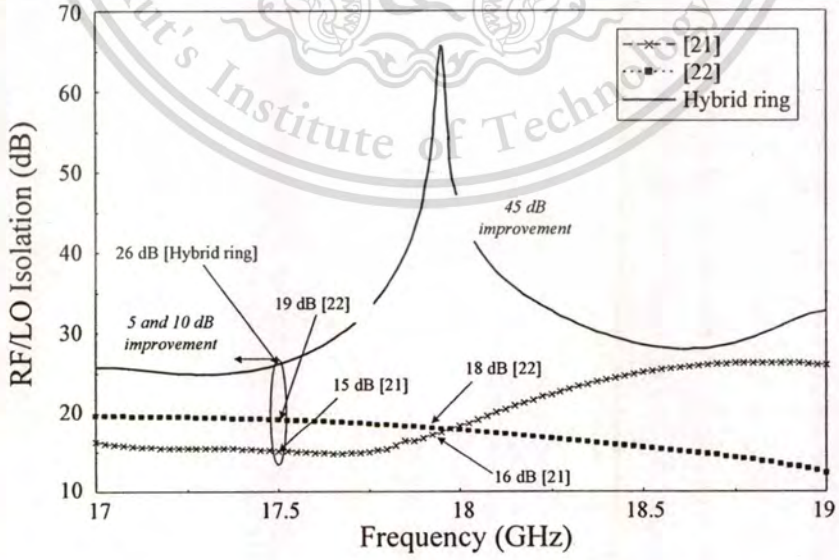

Fig. 3.5 Comparison of calculated RF/LO isolation of the hybrid ring coupler quasi-optical antenna-mixer with related works in [21] and [22]

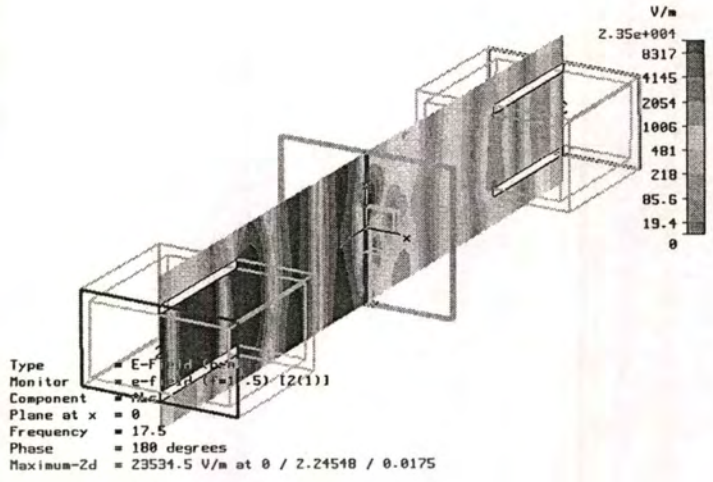

(a)

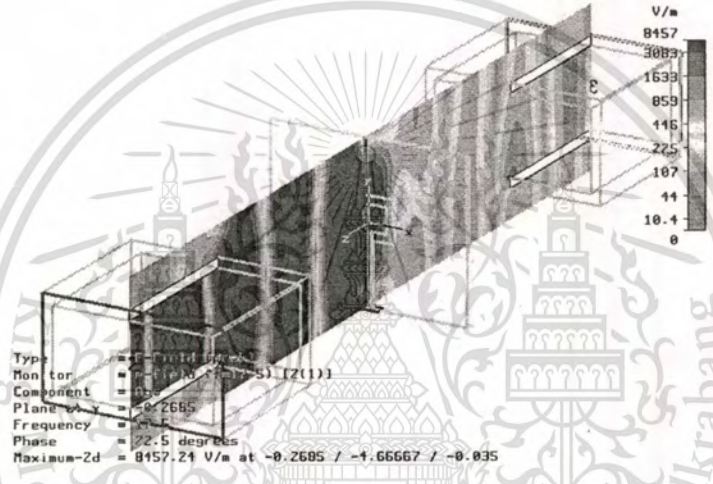

(b)

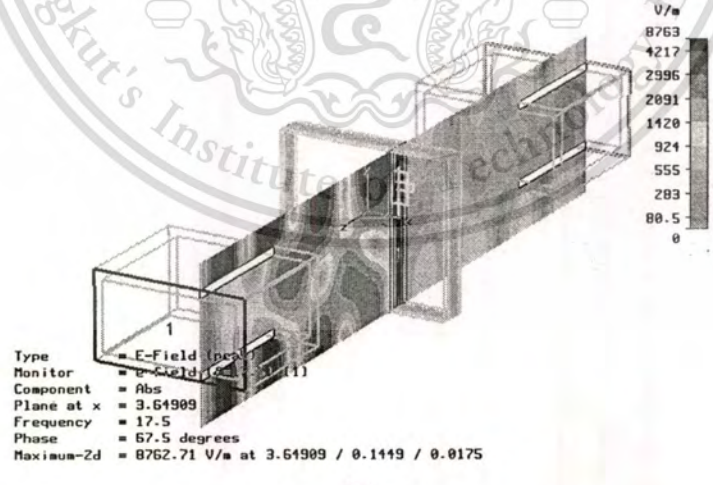

(c)

Fig. 3.6 Comparison of E-field in 2D of RF/LO isolation (a) A coplanar waveguide fed patch antenna (b) A magnetic loop antenna (c) A hybrid ring quasi-optical antenna-mixer

By comparing the isolation of the antennas in [21] and [22] in the frequency band of 17-19GHz with the proposed antenna, the results in Fig. 3.5 reveal that the proposed antenna can significantly improve isolation by 5-10dB at 17.5GHz.

Since the maximum isolation takes place at 17.95GHz, the significant improvement at this frequency is 45dB. It should be noted that the frequency of maximum isolation shifts from the desired frequency at 17.5GHz because the simulation by ADS2001^{TM} program neglected substrate dimension, ground plane size and air gap between the adjacent feeding stripline. The merit of improved isolation can be clarified as follows.

Comparison results of isolation by using CST2006 simulator are shown in Fig. 3.6 which shows the 2D of E-field in case of coplanar waveguide fed patch antenna, a magnetic loop antenna and a hybrid ring quasi-optical antenna-mixer. The magnitude of electric filed intensity is represented by colors from green (minimum) to red (maximum). These results clearly show that the E-field through port 1 to 2 (S_{21}) in Fig. 3.6(c) is less than Fig. 3.6(a) and (b). It should be confirmed that this hybrid ring quasi-optical antenna-mixer can be used to mitigate LO retransmitting signal.

3.5 Isolation and conversion loss measurement

By designing four quasi-optical antenna-mixers using the procedure in section 3.3 with the dimensions in Table 3.1 and Table 3.2, the RF frequency is 18.8GHz and the LO frequency is 17.5GHz. The fabricated antenna-mixers are shown in Fig. 3.7. Fig. 3.7(a), 3.7(b) and 3.7(c) show mixer circuit layer, ground plane-slot layer and patch antenna layer, respectively. The antenna was fixed by using plastic screws, and an aluminum tape was used to cover around the edge to prevent the LO signals coupling to the mixer circuits. The antenna spacing between elements was $0.9\lambda_{at\ 18.8\ GHz}$. The experimental setup for measuring the isolation is illustrated in Fig. 3.8(a). The isolation between LO transmitter and RF receiving antenna was measured by using an HP8510C network analyzer (S_{21}) with HP-P281C waveguide to coaxial adaptors. The distance between each side is 50mm to cover the far-field region. The absorber, using ECCOSORB® AN-77 Emerson, is used to cover the antenna side wall to prevent diffracted field. It is $10\lambda_{at\ 17\ GHz}$ extended from the edge of the quasi-optical antenna-mixers. Fig. 3.9(a) shows the isolation between LO to RF ports of the antenna-mixers

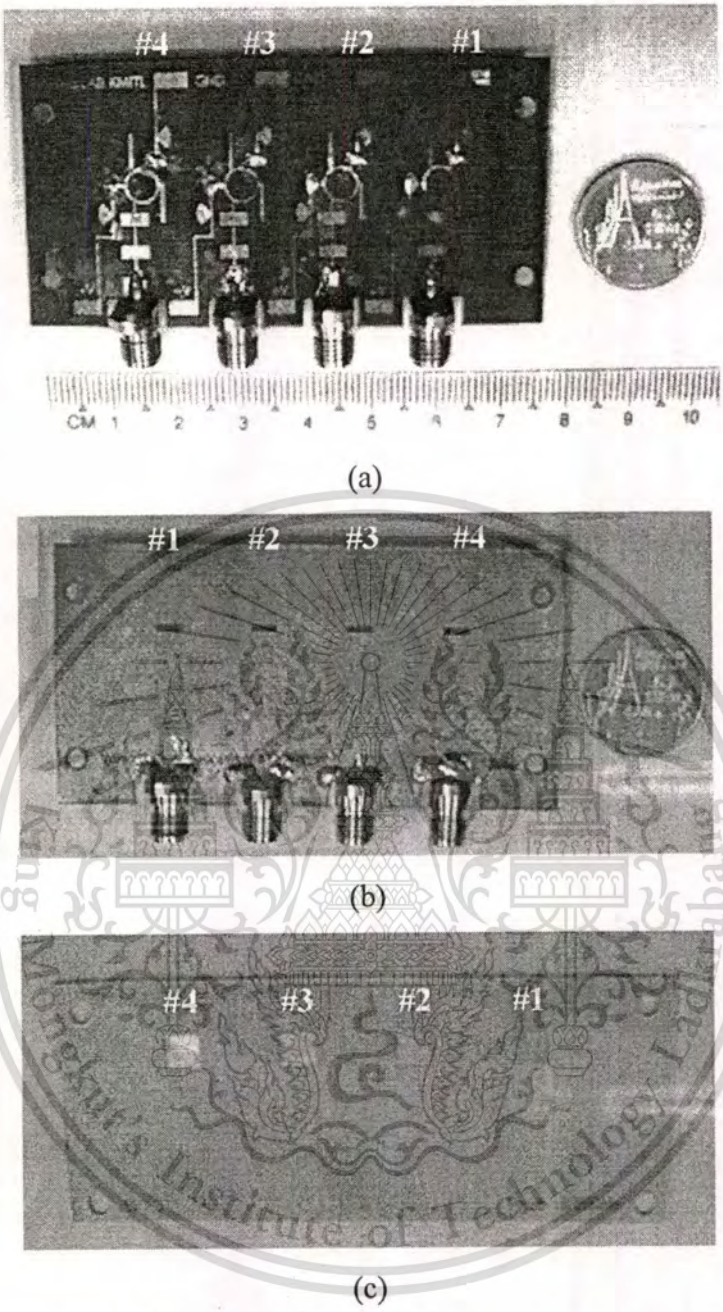

Fig. 3.7 Photographs of the fabricated quasi-optical antenna-mixers (a) Mixer circuit layer (b) Ground plane-slot layer (c) Patch layer

which show that the isolation of the elements number 1, 2, 3 and 4 are better than 35dB, 41dB, 41dB and 29dB, respectively. The corresponding frequencies are 18.37GHz, 18.28GHz, 18.33GHz and 18.19GHz, respectively. These values are markedly different from the simulation results in Fig. 3.5 since mixer diodes were assumed to be matched with $50\,\Omega$, and the mixer diodes need the air gap between the stripline and the upper feeding substrate in practical fabrication. The shifted frequency

from the designed frequency of 17.5GHz is around 0.8GHz which has an error of around 4.37%. These errors on isolation shifting and fluctuation will be discussed on mixer diodes biasing currents and LO pumping powers in the section 3.6.

The isotropic conversion loss of down converted signal (2.8) was measured by using an Agilent E4403B spectrum analyzer, an Agilent 83630B and an HP83640B sweep signal generator as shown in Fig. 3.8(b). The power levels of the RF and LO signals were set to the maximum value of +15dBm. Since, power level of the LO signal is not high enough to pump the Schottky diodes, a DC bias was added to optimize operation of this antenna-mixer. The biasing current was 1.658mA.

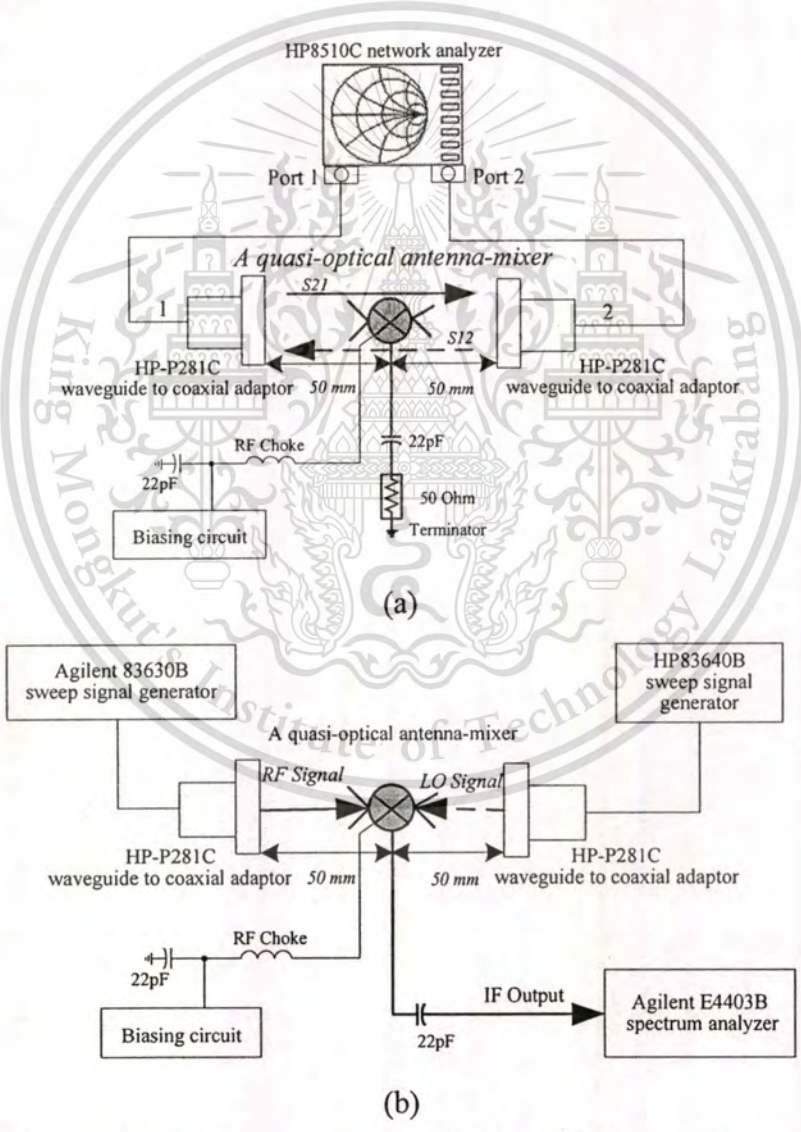

Fig. 3.8 Experimental setup (a) Isolation (b) Conversion loss

The isotropic conversion losses of the four antenna-mixers are shown in Fig. 3.9(b) which the conversion losses are better than 14dB (#2, #3) and 16dB (#1, #4) at

19.25GHz. The different conversion loss between outer antenna-mixer elements (#1, #4) and inner antenna-mixer elements (#2, #3) is due to non-uniform amplitude excitation of the LO signal, which the maximum is at the center of the antenna. The conversion losses of the proposed antenna are about 7 to 9dB higher than the conventional mixers [29]. The factor that strongly affects is the pumping local oscillator signal power level. The calculated local oscillator signal power level at the antenna-mixer was equal to -13.8dBm. Including the spill-over loss from the LO

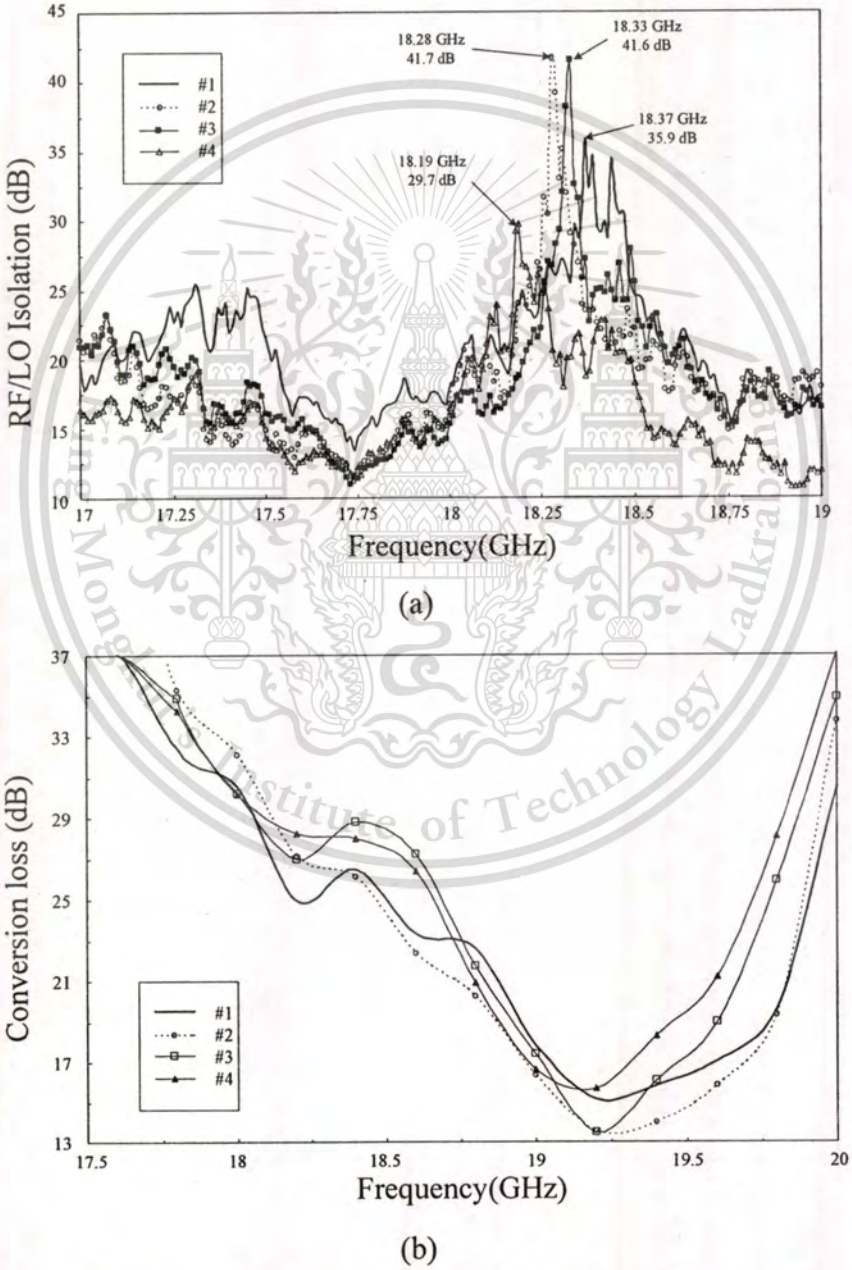

Fig. 3.9 Measured results versus frequency (a) RF/LO Isolation (b) Conversion loss

transmitting antenna of 5.6dB (found from radiated power of the TE_{10}-mode aperture antenna that illuminates the antenna-mixer divided by total radiated power), the total LO signal power level at the antenna-mixers is -19.4dBm. The frequency slightly shifts from 18.8GHz of the desired frequency with an error of 2.34%. The conversion loss is slightly higher than the conventional mixer due to the imperfect matching and DC series resistance in mixer diodes. These less measured errors ensure the accurate design procedure. It should be pointed out that the results of the four antenna-mixers are very close that guarantees the reproducibility of the fabrication.

3.6 Effect of mixer diodes biasing current and LO pumping power on isolation

It was found in the previous section that measured conversion loss is higher than the conventional mixers. The major contribution to this effect is the imperfect matching of the mixer diodes. This result can be improved by load-pull technique [34] which appropriate non-linear embedded impedance of the mixer diode can be selected by CAD software [35]. Since this work emphasizes on isolation improvement of quasi-optical antenna-mixer, this section will investigate on mixer diode biasing current and LO pumping power on isolation. Investigation was started by modeling the HSCH-9101 Schottky diode [36] as shown in Fig. 3.10. The model consists of an intrinsic model (SPICE: Bv=5V, Cjo=0.04pF, Eg=1.43, Xti=2, M=0.5, Is=1.6×10E-13A, Rs=5Ω, Ibv=10E-5A, Vj=0.7V and N=1.2) and an extrinsic model (package parasitic: Cp=35fF and Lp=0.1nH). The co-simulation of 3D electromagnetic simulation (CST2006^{TM}) and harmonic balance simulation (ADS2001^{TM}) was used for calculating isolation in term of embedded diode impedance that depends on DC biasing current and LO pumping power. We exported calculated S-parameters of the antenna structure with environmental setup as shown in Fig. 3.8(a) by CST2006^{TM}. Then, ports 1 and 2 were connected to the waveguides and ports 3, 4, 5 and 6 were connected to the diodes terminals depicted Fig. 3.1(b). The co-simulation setup is shown in Fig. 3.11.

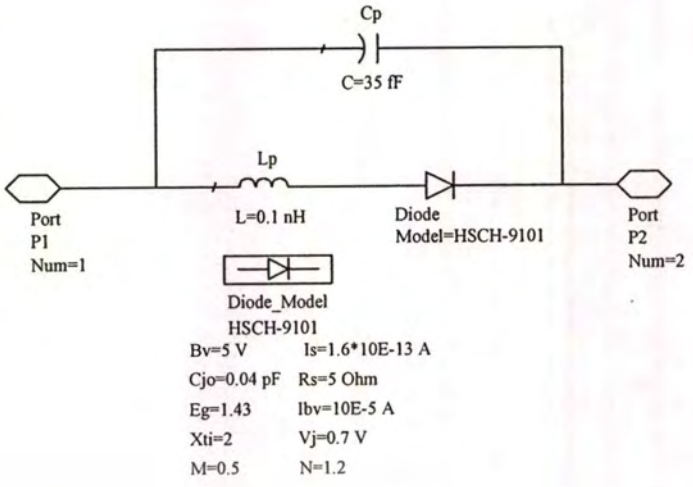

Fig. 3.10 Nonlinear microwave Schottky diode model

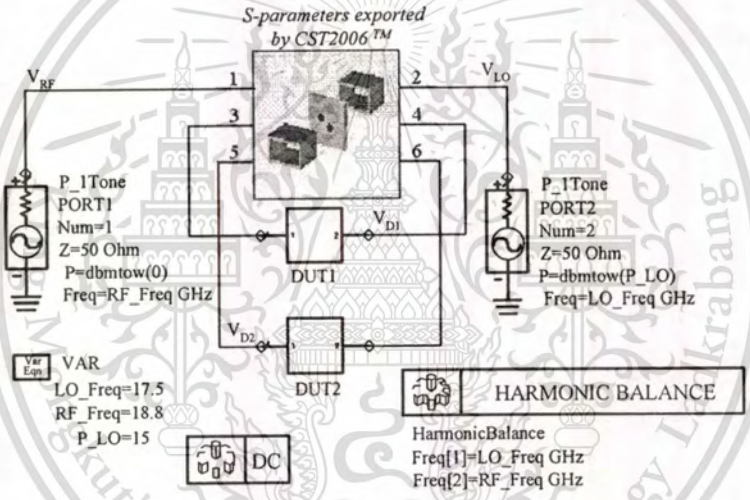

Fig. 3.11 Co-simulation of non-linear circuit and electromagnetic analysis setup

DUT1 and DUT2 represent diode models and biasing circuits (bias tees). LO frequency was swept from 17GHz to 18.8GHz to find isolation in this frequency band. The isolation was calculated from

$$Isolation(dB) = abs\left(dBm(HB.V_{RF}[::,1]) - dBm(HB.V_{LO}[::,1])\right) - P_L + G_{2A} \qquad (3.1)$$

where $dBm(HB.V_{RF}[::,1])$ is LO power at V_{RF} and $dBm(HB.V_{LO}[::,1])$ is LO pumping power at V_{LO}. P_L and G_{2A} are path loss and gain of the used waveguides. These quantities vary as the frequency is changed. The first simulation utilized LO pumping

power (P_{LO}) of +15dBm. It was found that LO pumping power at the points V_{D1} and V_{D2} were -18.7dBm. This value takes path loss, spillover loss and mismatch of mixer diodes into account. The values of RF/LO isolations at 17.95GHz, shown in Fig. 3.12, for the biasing currents of 0mA, 1.658mA, 5mA, 10mA and 20mA are 59.2dB, 51.6dB, 47.2dB, 46.4dB and 46.1dB, respectively. It is noted that isolation and bandwidth are inversely proportional to biasing current.

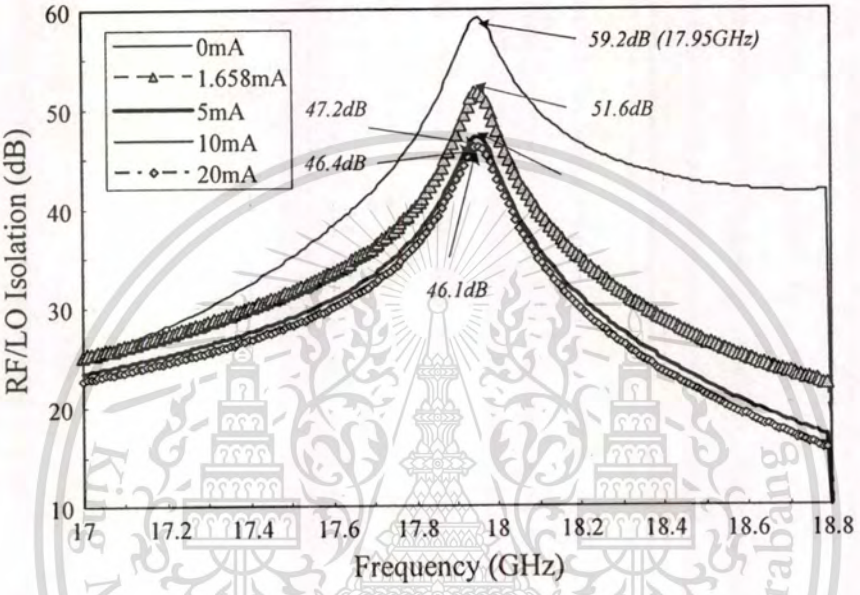

Fig. 3.12 RF/LO isolation versus biasing currents

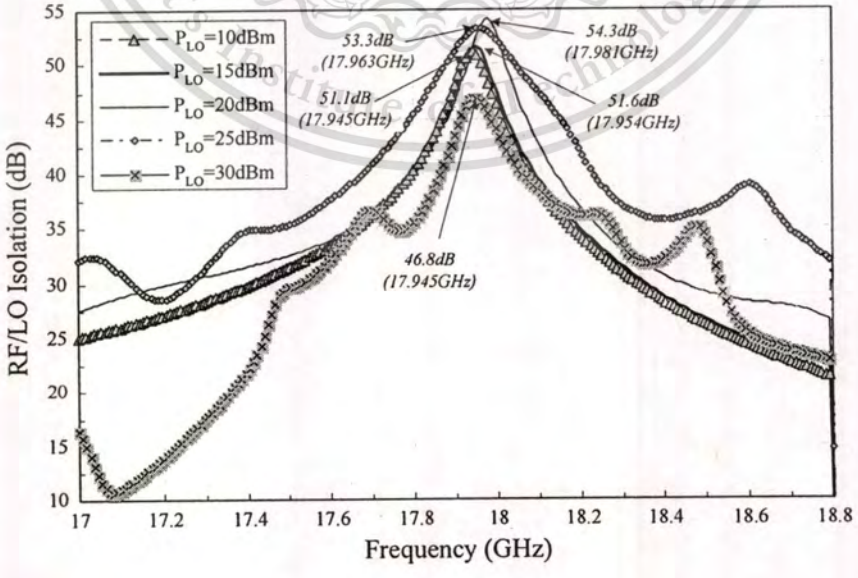

Fig. 3.13 RF/LO isolation versus LO pumping power levels

The second simulation was conducted when biasing current was 1.658mA corresponding to the measured minimum conversion loss. The LO pumping power was varied from +10dBm (P_{LO} at $V_{DI,2}$=-23.8dBm), +15dBm (P_{LO} at $V_{DI,2}$=-18.7dBm), +20dBm (P_{LO} at $V_{DI,2}$=-13.3dBm), +25dBm (P_{LO} at $V_{DI,2}$=-6.2dBm) and +30dBm (P_{LO} at $V_{DI,2}$=1.4dBm). The results are shown in Fig. 3.13, which can be observed that isolation increases as LO pumping power is increased from +10dBm to +20dBm. The isolations when LO pumping power of +10dBm, +15dBm and +20dBm are 51.1dB, 51.6dB and 54.3dB, respectively. Saturation takes place at the LO pumping power of +20dBm, then isolation decreases as LO pumping power is increased. The corresponding isolations at LO pumping power of +25dBm and +30dBm are 53.3dB and 46.8dB, respectively. The frequency at maximum isolation deviates from 17.945GHz to 17.981GHz due to large-signal effects [37]. It should be noted that the shape of the isolation versus frequency curves when LO pumping power are +25dBm and +30dBm are different from the conventional smooth curve due to intermodulation.

From these two simulations, the diode biasing current and LO pumping power must be appropriately designed to provide good isolation. Furthermore, conversion loss can be improved by utilizing the load-pull technique. Measurement results differ from the simulation ones can be criticized as follows. The shift of frequency that maximum isolation takes place belongs to the hybrid rings' radii manufacturing error as can be clearly depicted in Fig. 3.2. The measured isolation is markedly less than the simulated one due to the measured diode model is different from the one in simulation. Performance of the proposed antenna can be accurately realized by taking this effect into account and utilizing more accurate fabrication process.

3.7 Conclusion

A hybrid ring coupler antenna-mixer is proposed to improve RF/LO isolation. It consists of an aperture-coupled inverted square patch for receiving RF and LO signals and a hybrid ring with mixer diodes for signal mixing. The hybrid ring quasi-optical antenna-mixer was analyzed and it was found that a hybrid ring radius has a sensitive effect on RF/LO isolation. A slot length (l_{ar}) should be longer than a patch width (l_p) to obtain wide bandwidth. The proposed antenna-mixer provides significant RF/LO

isolation compared with the conventional ones. The effect of RF/LO isolation on error in IF output signal has been illustrated. A four-element hybrid ring coupler quasi-optical antenna-mixer was designed to operate at K-band and tested. It provides around 29dB RF/LO isolation and 16dB conversion loss with 4.37% frequency shift from the desired frequency. This high isolation quasi-optical antenna-mixer can be applied in an inverse measurement technique for dielectric property determination. The detail will be shown in chapter 6.

CHAPTER 4
A MULTIBEAM ANTENNA USING QUASI-OPTICAL ANTENNA-MIXER ARRAY

4.1 Introduction

The design and demonstration of a multibeam antenna using quasi-optical antenna-mixer array are presented in this chapter. This antenna can scan the mainbeam by controlling the LO's incoming incident angle. In the system like Multiple Input Multiple Output (MIMO) system and pattern diversity systems, the used antenna has to provide multiple beams simultaneously. In order to produce a multibeam antenna without a complicated feeding system, this chapter presents the use of quasi-optical antenna-mixers whose LO transmitters at different frequencies are used to provide multibeam at different IF frequencies. By taking element patterns into account, accurate beam directions can be accomplished. This kind of multibeam antenna is useful for modern wireless communications.

4.2 Principle of a multibeam antenna using quasi-optical antenna-mixers

A multibeam antenna was designed based on the principle of quasi-optical antenna mixers. By using the beam scanning principle that was described in chapter 2, the mainbeam of the antenna can be scanned by changing the LO direction and the LO frequency without using phase shifters. In this chapter, this method is used to demonstrate a multibeam antenna which is achieved by using three LO transmitting signals instead of one LO signal. Fig. 4.1 shows the proposed multibeam antenna. The configuration of the multibeam antenna using quasi-optical hybrid ring antenna-mixer array is shown in Fig. 4.1(a). Fig. 4.1(b) shows the top view of the mixer circuits and the 6 layers cross-section of quasi-optical antenna-mixer element. To scan the mainbeam, the direction of the RF receiving beam at the lower side of the antenna is defined by the direction of the LO transmitting antenna at the upper side. The multibeam operation is realized by using different LO frequencies with different resultant intermediate frequencies.

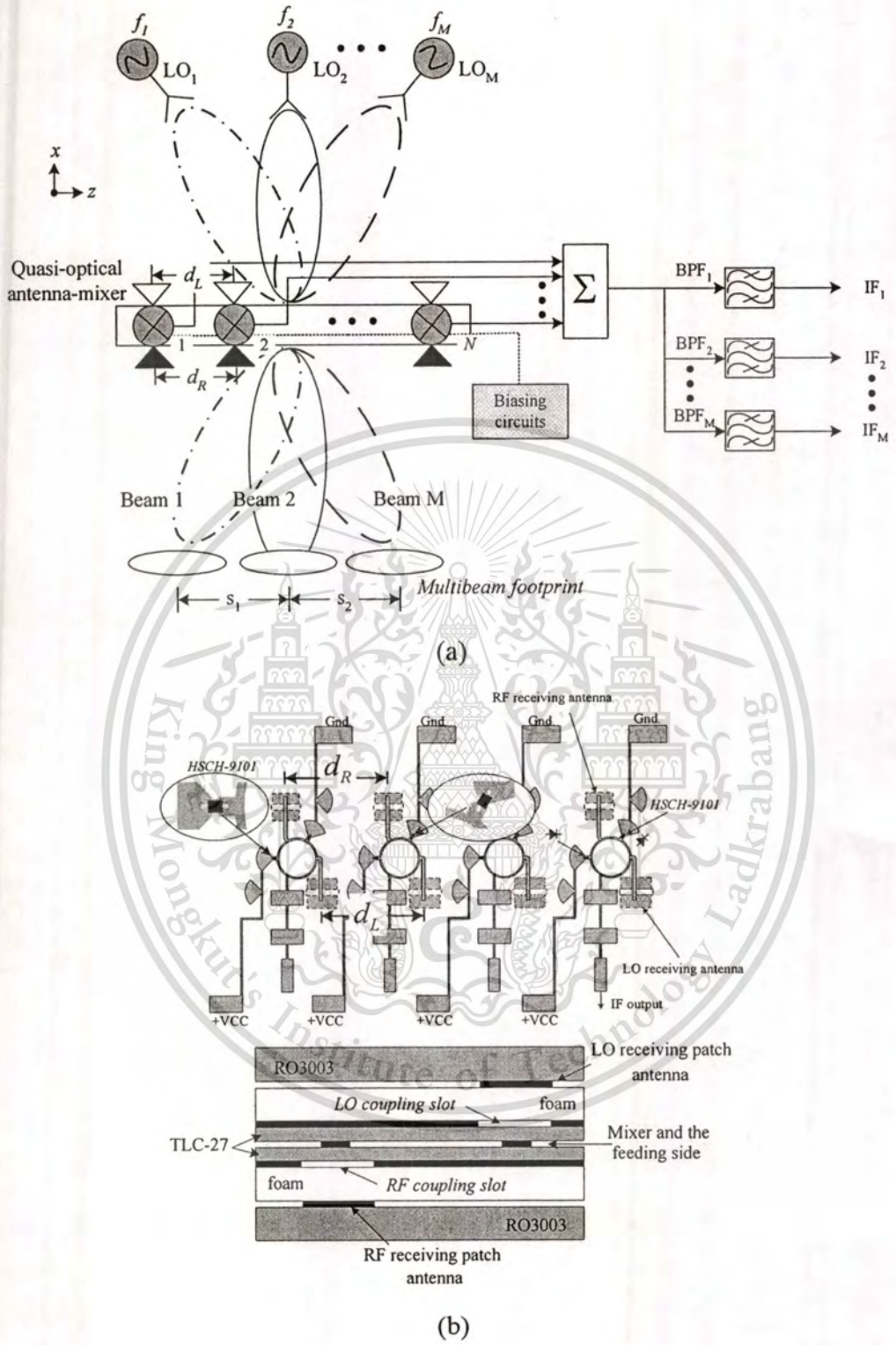

Fig. 4.1 A multibeam antenna using quasi-optical antenna-mixers (a) Configuration (b) Top view of mixer circuits and cross-section of the quasi-optical antenna-mixer

For a linear array of N elements, radiation pattern of the down converted intermediate frequency signals on XZ plane from M LO's can be presented as IF_{SUM}.

$$IF_{SUM} = RF \otimes (LO_1 + LO_2 + \ldots LO_M)$$

$$= [RF \otimes LO_1] + [RF \otimes LO_2] + \ldots [RF \otimes LO_M] \tag{4.1}$$

where $RF = A_R(\theta)\cos(\omega_R t - \varphi_R)$ and $LO = A_L(\theta)\cos(\omega_L t - \varphi_L)$. From $\cos A \cdot \cos B = 0.5[\cos(A-B) + \cos(A+B)]$, equation (4.1) becomes

$$IF_{SUM} = A_R(\theta)\cos(\omega_R t - \varphi_R) \otimes \begin{bmatrix} A_{L1}(\theta)\cos(\omega_{L1} t - \varphi_{L1}) \\ +A_{L2}(\theta)\cos(\omega_{L2} t - \varphi_{L2})] \\ \vdots \\ +A_{LM}(\theta)\cos(\omega_{LM} t - \varphi_{LM}) \end{bmatrix}$$

$$= \begin{Bmatrix} 0.5A_R(\theta)A_{L1}(\theta)\left[\cos\left((\omega_R - \omega_{L1})t - (\varphi_R - \varphi_{L1})\right)\right] \\ +0.5A_R(\theta)A_{L1}(\theta)\left[\cos\left((\omega_R + \omega_{L1})t + (\varphi_R + \varphi_{L1})\right)\right] \\ +0.5A_R(\theta)A_{L2}(\theta)\left[\cos\left((\omega_R - \omega_{L2})t - (\varphi_R - \varphi_{L2})\right)\right] \\ +0.5A_R(\theta)A_{L2}(\theta)\left[\cos\left((\omega_R + \omega_{L2})t + (\varphi_R + \varphi_{L2})\right)\right] \\ \vdots \\ +0.5A_R(\theta)A_{LM}(\theta)\left[\cos\left((\omega_R - \omega_{LM})t - (\varphi_R - \varphi_{LM})\right)\right] \\ \vdots \\ +0.5A_R(\theta)A_{LM}(\theta)\left[\cos\left((\omega_R + \omega_{LM})t + (\varphi_R + \varphi_{LM})\right)\right] \end{Bmatrix}. \tag{4.2}$$

When the up converted signals are filtered out, equation (4.2) is reduced to the down converted signals:

$$IF_{SUM} = \begin{Bmatrix} 0.5A_R(\theta)A_{L1}(\theta)\left[\cos\left((\omega_R - \omega_{L1})t - (\varphi_R - \varphi_{L1})\right)\right] \\ +0.5A_R(\theta)A_{L2}(\theta)\left[\cos\left((\omega_R - \omega_{L2})t - (\varphi_R - \varphi_{L2})\right)\right] \\ +\ldots 0.5A_R(\theta)A_{LM}(\theta)\left[\cos\left((\omega_R - \omega_{LM})t - (\varphi_R - \varphi_{LM})\right)\right] \end{Bmatrix}. \quad (4.3)$$

Moreover, the phase references $(\varphi_R - \varphi_{L1,2\ldots M})$ are modified to the phase of an array factor including radiation patterns of patch antennas. Hence, equation (4.3) becomes

$$IF_{SUM} = \begin{Bmatrix} 0.5\cos(\omega_R - \omega_{L1})t \times A_R(\theta)A_{L1}(\theta)\sum_{i=1}^{N}\left[e^{j(N-1)(k_R d_R \cos\theta_R - k_{L1} d_{L1}\cos\theta_{L1})}\right] \\ +0.5\cos(\omega_R - \omega_{L2})t \times A_R(\theta)A_{L2}(\theta)\sum_{i=1}^{N}\left[e^{j(N-1)(k_R d_R \cos\theta_R - k_{L2} d_{L2}\cos\theta_{L2})}\right] \\ \vdots \\ +0.5\cos(\omega_R - \omega_{LM})t \times A_R(\theta)A_{LM}(\theta)\sum_{i=1}^{N}\left[e^{j(N-1)(k_R d_R \cos\theta_R - k_{LM} d_{LM}\cos\theta_{LM})}\right] \end{Bmatrix} \quad (4.4)$$

where $A_R(\theta)$ and $A_{L1,L2,\ldots LM}(\theta)$ are H-plane radiation patterns of the microstrip patch antennas of the RF and LO receiving antennas, respectively. M is the number of elements, k_R is the wave number of the RF signal, k_L is the wave number of the LO signal , d_R is the separation between elements of RF receiving patch antennas, and d_L is the separation between elements of LO receiving patch antennas. d_R and d_L are generally different, but they can be same in practical. The H-plane of radiation pattern of patch antenna using the cavity model can be calculated by [30]

$$H_{(\theta)\text{single element}} = j\frac{2V_0 e^{-jk_0 r}}{\pi r}\left[\sin\theta\frac{\sin\left(\frac{k_0 W}{2}\cos\theta\right)}{\cos\theta}\right]\cos\left(\frac{k_0 L}{2}\sin\phi\right) \quad (4.5)$$

where W is a patch width, L is a patch length, and r is an observation point (far field region). The directions of RF and LO signals are depicted by θ_R and θ_L, respectively. By varying the LO transmitting antenna direction and frequency, Fig. 4.2 shows relation of mainbeam directions to LO directions for RF of 18.8 GHz when isotropic sources and patch antennas are used. It is noted that the relation fluctuates instead of

linear relationship when the patch antennas are used instead of the isotropic sources. This effect is due to the pattern multiplication of an array factor with patch radiation patterns. Fig. 4.3 shows the pattern multiplication between array factor and radiation pattern of patch antenna when $d_R = d_L = 0.5\lambda_R$, $f_{LO} = 17.5$ GHz, and $\theta_L = -20$ degrees.

Form calculation results, when the mainbeam direction of array factor is at -20°, the H-plane radiation pattern of patch has maximum at 0°. Therefore, the mainbeam results from pattern multiplication will be at -18°. The beam direction, normally depends on the direction of the LO transmitting antenna (θ_L) and LO frequency (f_L), is limited by non-isotropic radiation patterns such as patch antenna, the distance between antenna elements and the difference between RF and LO frequencies (f_L). It is noted in Fig. 4.2 that LO direction has more pronounced effect on mainbeam direction than LO frequency. Therefore, it is important to carefully specify the LO direction.

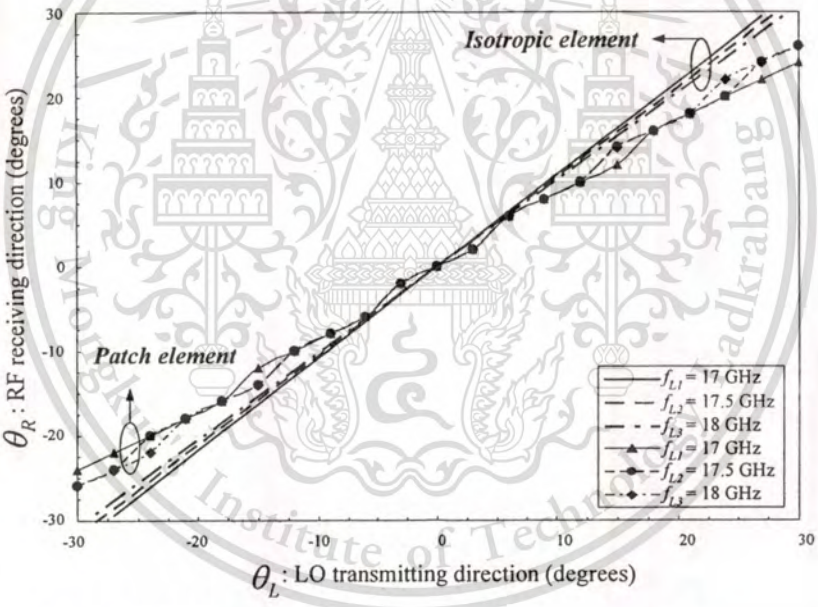

Fig. 4.2 Relation of mainbeam direction to LO direction

4.3 Experimental results

To demonstrate the multibeam operation, a 4×1 quasi-optical hybrid ring antenna-mixer was fabricated as shown in Fig. 4.4. Fig. 4.4(a) shows hybrid ring mixers on feeding side and Fig. 4.4(b) shows the mixer circuit using HSCH-9101 Schottky diodes. Experimental setup for multibeam operation is shown in Fig. 4.4(c). The distance between antenna elements was $0.9\,\lambda_{at18.8GHz}$. It was limited by the hybrid

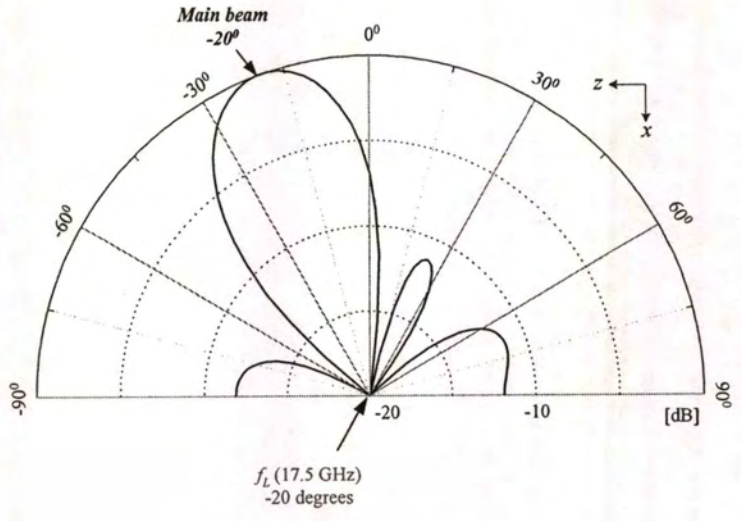

(a)

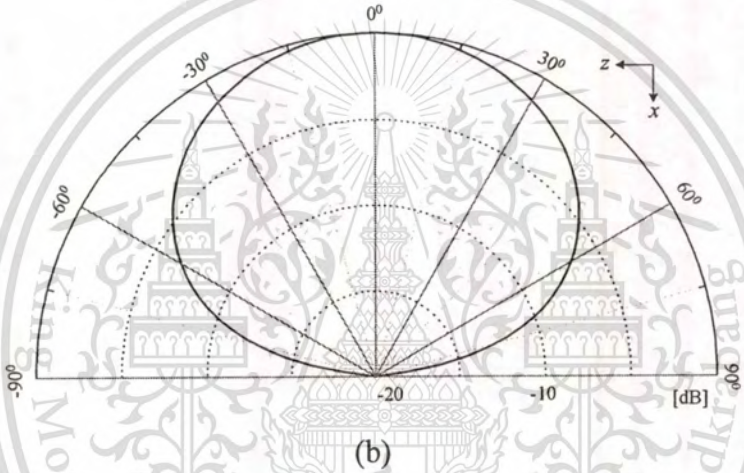

(b)

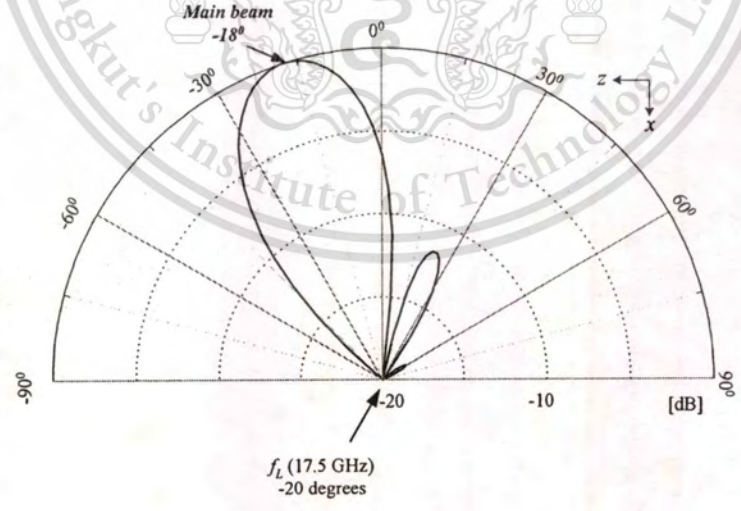

(c)

Fig. 4.3 Pattern multiplication (a) Array factor (b) Patch antenna element (c) Total radiation pattern

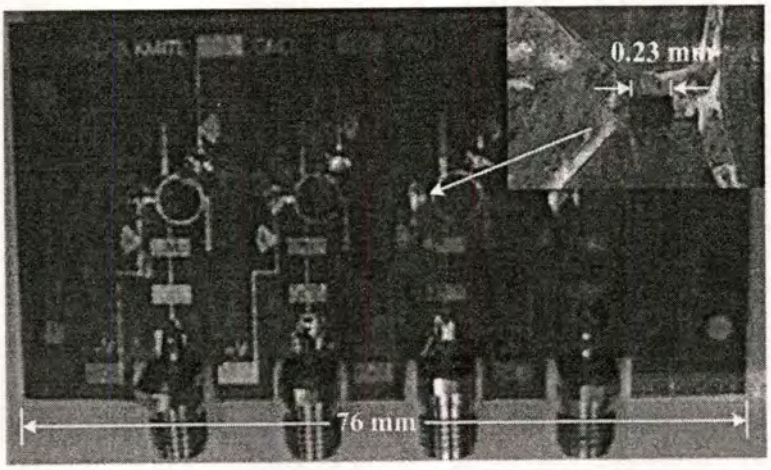

(a)

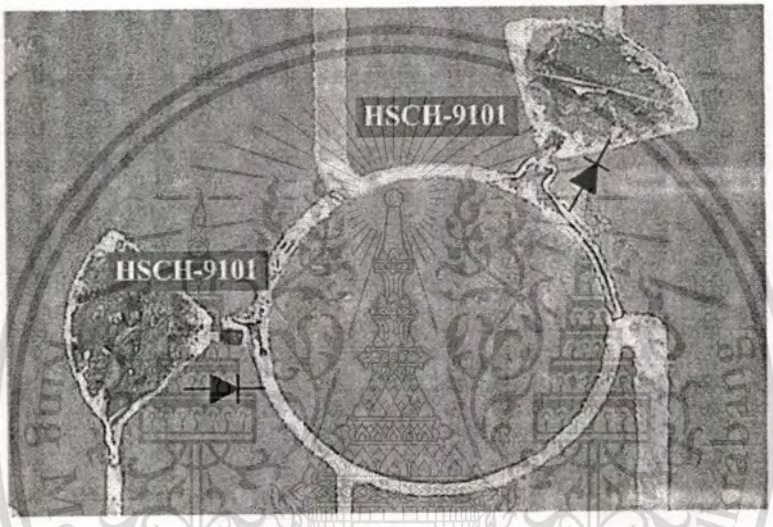

(b)

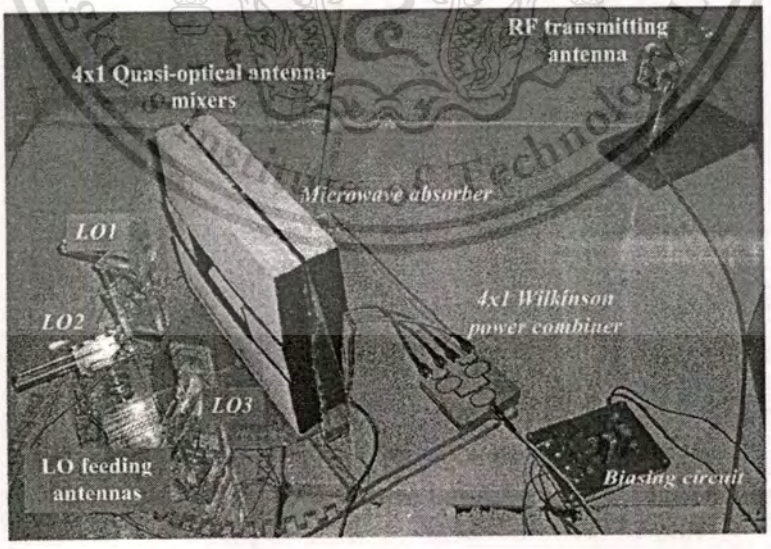

(c)

Fig. 4.4 Photographs of the fabricated multibeam antenna (a) Hybrid ring mixers on feeding side (b) Mixer circuit (c) Experimental setup for multibeam operation

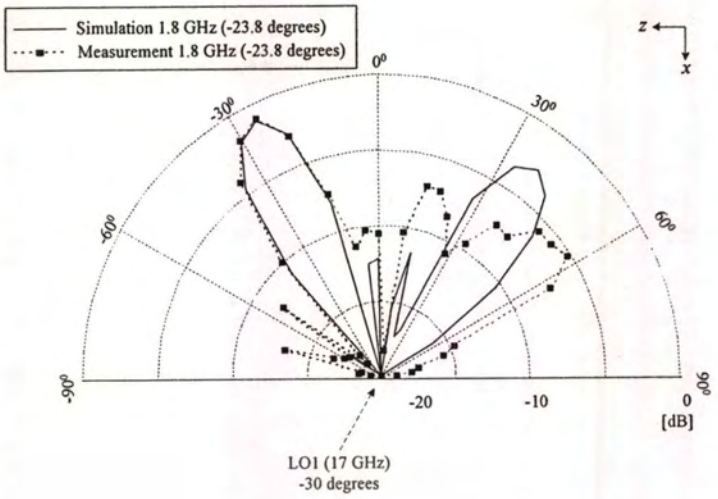

(a)

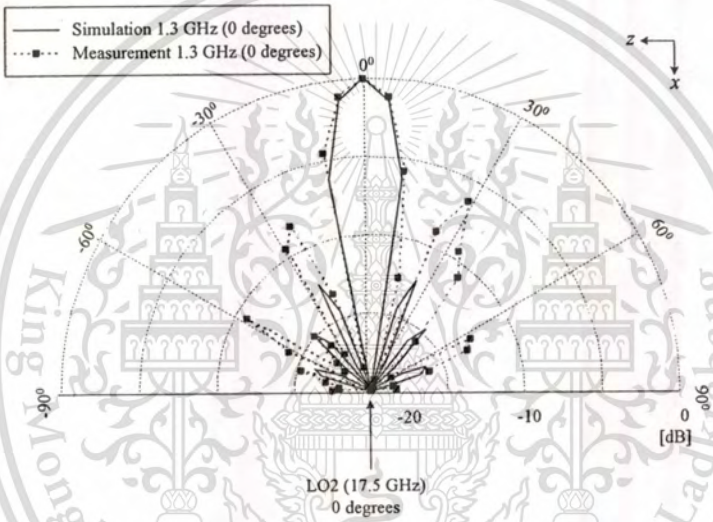

(b)

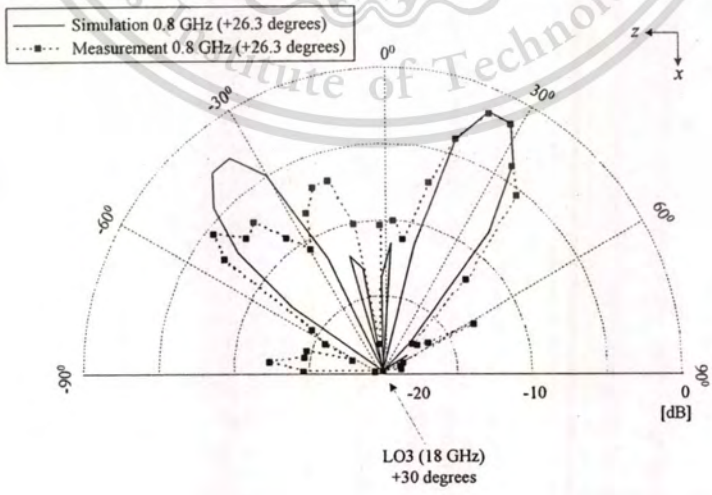

(c)

Fig. 4.5 Multibeam radiation patterns (a) Beam 1 at -23.8 degrees (b) Beam 2 at 0 degrees (c) Beam 3 at +26.3 degrees

ring coupler dimension. Each LO signal was produced by using a tilted active patch antenna placed at three positions. The three active patch antennas were placed at -30°, 0° and +30° off broadside to feed LO signals at 17 GHz (LO1), 17.5 GHz (LO2) and 18 GHz (LO3) for multibeam demonstration. The IF power of each element was calibrated by adjusting biasing current to obtain uniform amplitude excitation. The radiation patterns are shown in Fig. 4.5 which demonstrates three beam operations at the same time. The results were measured at 1.8 GHz (Beam1), 1.3 GHz (Beam2) and 0.8 GHz (Beam3) as shown in Fig. 4.5(a), Fig. 4.5(b) and Fig. 4.5(c), respectively. The measured mainbeam directions agree well with the calculated patterns. However, the side lobe levels were different because calculation in (4.4) neglected mutual coupling effect and non-uniform LO amplitude excitation due to the fabrication process. Grating lobes took place due to wide separation of antenna elements. To analyze the effect of antenna separation on side lope level (SLL), the predicted SLL is illustrated in Fig 4.6 when antenna separation and LO transmitting frequencies are varied. Simulated patterns of the proposed antenna with d_R = 0.5λ, 0.7λ and 0.9λ are illustrated. The corresponding side lobes are -13 dB, -7 dB and -3dB down from the main lobe, respectively. It is obvious that side lobe could be reduced further by reducing separation between antenna elements. It can be improved by reducing hybrid ring size [38].

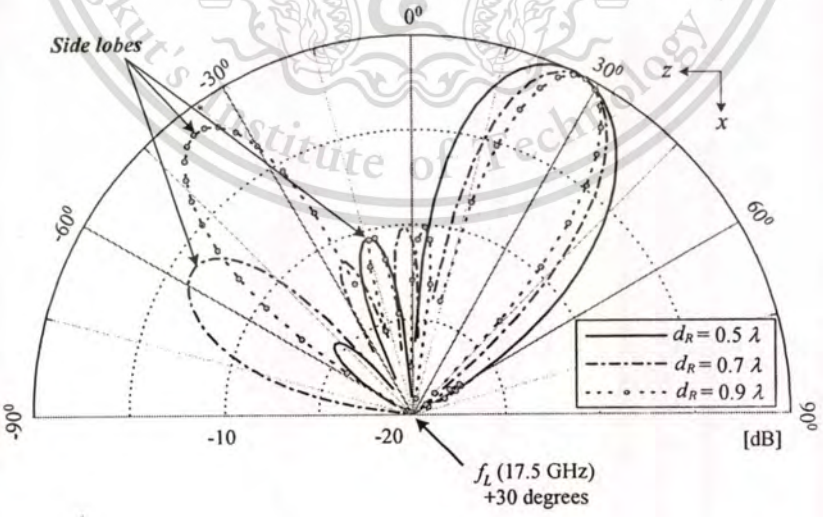

Fig. 4.6 Simulated patterns at different d_R

4.4 Conclusion

A multibeam antenna using quasi-optical antenna-mixers is presented in this chapter. The accurate RF receiving mainbeam direction can be obtained when the patch antenna patterns are taken into account. The results show three receiving mainbeams which can be used in multibeam operation. A multibeam antenna can be designed without using a complicated feeding system by using quasi-optical antenna-mixers. Accurate beam directions could be obtained when practical antenna patterns was taken into account in the design. The effectiveness of a three-beam antenna is demonstrated at K-band showing accurate beam directions which is very useful in modern wireless communications.

CHAPTER 5

RADIATION PATTERN OF A QUASI-OPTICAL ANTENNA-MIXER ARRAY FED BY NON-UNIFORM PLANE WAVE

5.1 Introduction

This chapter presents an effect of non-uniform plane wave on radiation pattern of a quasi-optical antenna-mixer array. Amplitude and phase excitation of the quasi-optical antenna-mixer array that takes non-uniform of plane wave illuminated on each element have been formulated. Simulation results show main beam squint and side lobe level error in term of number of elements. The results show examples of error of radiation patterns of the quasi-optical antenna-mixer array fed by a non-uniform plane wave local oscillator. The result of this study provides the more accurate design of this antenna.

5.2 Formulation

The diagram of a quasi-optical antenna-mixer array is shown in Fig. 5.1. The quasi-optical antenna-mixer elements are placed on the z-axis, and the RF signal incidents on the upper side of the quasi-optical antenna-mixers. The LO transmitting antenna for transmitting LO signals is placed on the z'-axis in the far-field range and it has an isotopic radiation pattern. The received RF (Radio Frequency) signal is transformed to IF signal at each array element and are combined at a power combiner. The obtained IF signal of the nth element is

$$IF = E_{R(n)} \cos(\omega_R t + n\varphi_R) \otimes E_{L(n)} \cos(\omega_L t + n(\varphi_L + \phi_L)) \tag{5.1}$$

where $E_{R(n)}$ and $E_{L(n)}$ are amplitudes of the RF and LO receiving signals, respectively. ω_R is an angular frequency of the RF signal and ω_L is the angular frequency of the

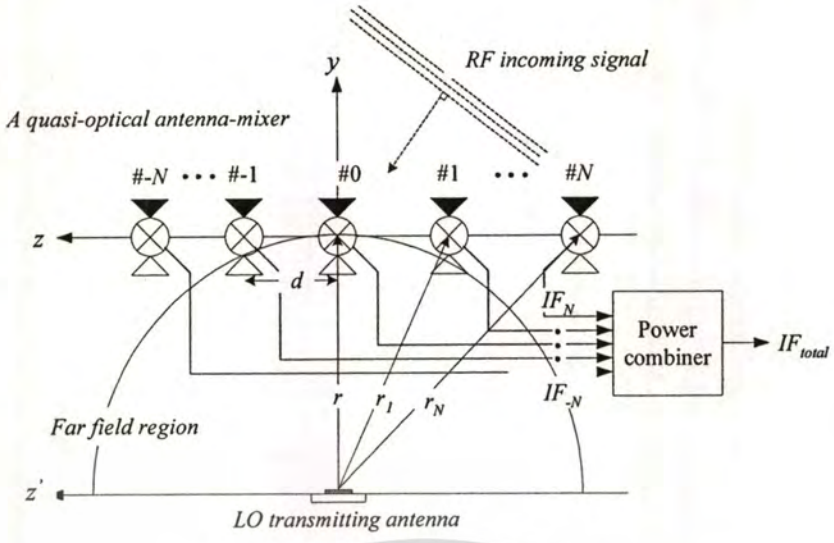

Fig. 5.1 Diagram of quasi-optical antenna-mixer array

LO signal. $n\phi_L$ is the progressive phase delay of the non-uniform plane wave of the LO signal, then

$$IF = 0.5K_n E_{R(n)} E_{L(n)} \times \left[\begin{array}{l} \left(\cos((\omega_R t + n\varphi_R) - (\omega_L t + n(\varphi_L + \phi_L)\right) \\ +\left(\cos((\omega_R t + n\varphi_R) + (\omega_L t + n(\varphi_L + \phi_L)\right) \end{array} \right] \quad (5.2)$$

where K_n is the conversion gain of the mixer. Therefore,

$$IF = 0.5K_n E_{R(n)} E_{L(n)} \times \left[\begin{array}{l} \cos(\omega_R t + n\varphi_R - \omega_L t - n(\varphi_L + \phi_L)) \\ +\underline{\cos(\omega_R t + n\varphi_R + \omega_L t + n(\varphi_L + \phi_L))} \end{array} \right]. \quad (5.3)$$

For down conversion, $\underline{\cos(\omega_R t + n\varphi_R + \omega_L t + n(\varphi_L + \phi_L))}$ can be omitted and the IF signal is reduced to

$$IF = 0.5K_n E_{R(n)} E_{L(n)} \times \cos((\omega_R - \omega_L)t - n(\varphi_R - (\varphi_L + \phi_L))) . \quad (5.4)$$

Consideration of the linear array geometry in Fig. 5.1, summation of IF signals from all elements provide the total signal, I_{Total} .

$$IF_{Total} = 0.5k_n A_R \cos(\omega_R - \omega_L)t \times$$

$$\sum_{i=1}^{N}\left[A_{L(i-1)}\times e^{j(i-1)(k_R d\cos\theta_R-(k_L d\cos\theta_L+\phi_{L(i-1)}))}\right]. \quad (5.5)$$

The normalized total IF signal is presented as I_{TotalN}.

$$IF_{TotalN}=\cos(\omega_R-\omega_L)t\times \sum_{i=1}^{N}\left[A_{L(i-1)}\times e^{j(i-1)(k_R d\cos\theta_R-(k_L d\cos\theta_L+\phi_{L(i-1)}))}\right] \quad (5.6)$$

Referring to Fig. 5.1, the non-uniform LO amplitude and phase excitation can be determined from the different propagation paths from the LO transmitting antenna to each element of the array. The free space loss and phase shift are different. The amplitude and phase excitation of each array element for the array of odd number of elements can be expressed in (5.7) and (5.8), respectively.

$$A_L(odd)=\frac{r}{\sqrt{r^2+(nd)^2}} \quad (5.7)$$

$$\phi_L(odd)=k\left(\sqrt{r^2+(nd)^2}-r\right) \quad (5.8)$$

where r and d are the distance between the LO transmitting antenna to the quasi-optical antenna-mixer array (far-field region) and the separation between antenna-mixer elements, respectively. The amplitude and phase excitations of the array with even number of elements are in (5.9) and (5.10), respectively.

$$A_L(even)=\frac{r}{\sqrt{(0.5\times(2n-1)d)^2+r}} \quad (5.9)$$

$$\phi_L(even)=k\left[\sqrt{r^2+(0.5\times(2n-1)d)^2}-r\right] \quad (5.10)$$

5.3 Simulation results

To demonstrate the effect of non-uniform LO signal excitation, it is assumed that there is no coupling between quasi-optical antenna-mixer elements. The LO transmitting distance (r) is assumed to be in the far-field region ($10D^2/\lambda$) where D is the largest LO transmitting antenna dimension (0.5λ). The separation between antenna elements (d) is 0.5λ. The amplitude and phase excitation of each element in arrays of different number of elements, by using proposed formulation are tabulated in Table 5.1.

Table 5.1 Amplitude and phase excitation of the array (A: Normalized amplitude, ϕ: phase in degree)

N	0	±1	±2	±3	±4	±5	±6	±7	±8	±9	±10
2	-	0.9, 4.5^o	-	-	-	-	-	-	-	-	-
11	1, 0^o	0.9, 4.4^o	0.9, 7.0^o	0.8, 9.9^o	0.7, 13^o	0.7, 19^o	-	-	-	-	-
20	-	0.9, 4.5^o	0.9, 5.7^o	0.8, 8.5^o	0.8, 11^o	0.7, 14^o	0.7, 18^o	0.7, 21^o	0.6, 24^o	0.6, 27^o	0.6, 30^o

Table 5.2 Amplitude and phase excitation of the array by CST2006^{TM} (A: Normalized amplitude, ϕ: phase in degree)

N	0	±1	±2	±3	±4	±5	±6	±7	±8	±9	±10
2	-	0.9, 7.8^o	-	-	-	-	-	-	-	-	-
11	1, 0^o	0.9, 5.6^o	0.9, 9.4^o	0.8, 10.8^o	0.7, 17^o	0.6, 25^o	-	-	-	-	-
20	-	0.9, 7.8^o	0.9, 9.9^o	0.8, 11.7^o	0.7, 14.8^o	0.7, 18^o	0.6, 23^o	0.6, 28^o	0.6, 31^o	0.5, 37^o	0.5, 42^o

Table 5.2 shows the relatively simulated amplitude and phase excitation by CST2006^{TM} commercial software. We used the dipole because it has omni-directional radiation pattern in H-plane. The model comprises of the half-wave length dipole (7.3 mm), the 0.4 mm gap distance and 0.5 mm of dipole diameter. The simulated models are calculated in case of 2 elements, 11 elements and 20 elements, respectively. Fig. 5.3 shows 2D of E-field of half-wave length dipole by CST2006^{TM} model. It should

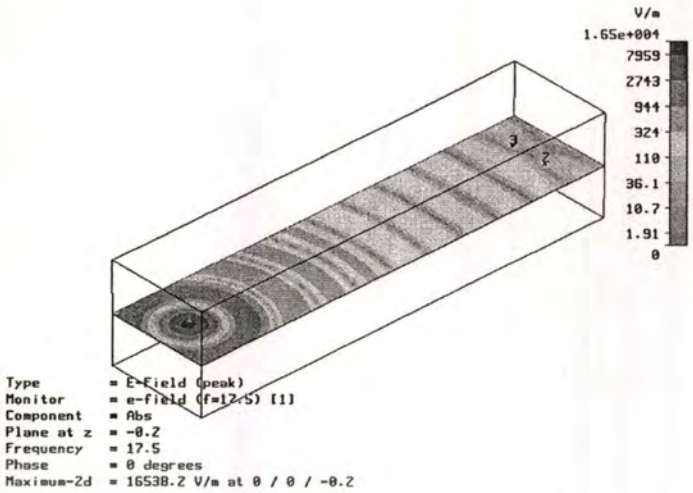

(a)

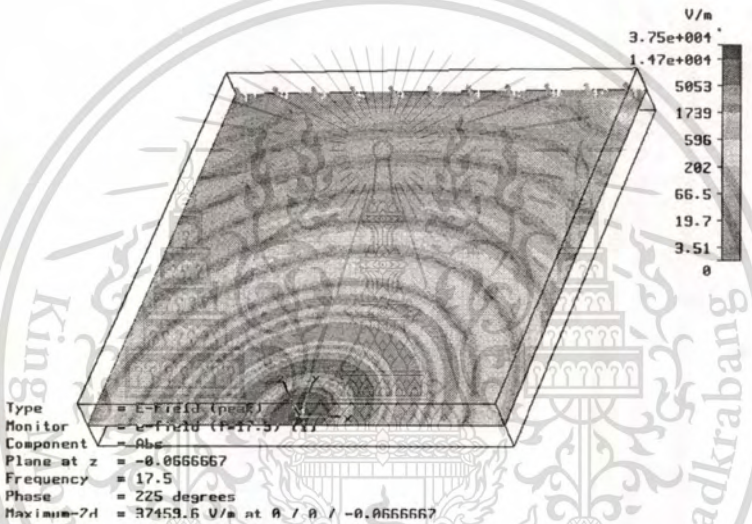

(b)

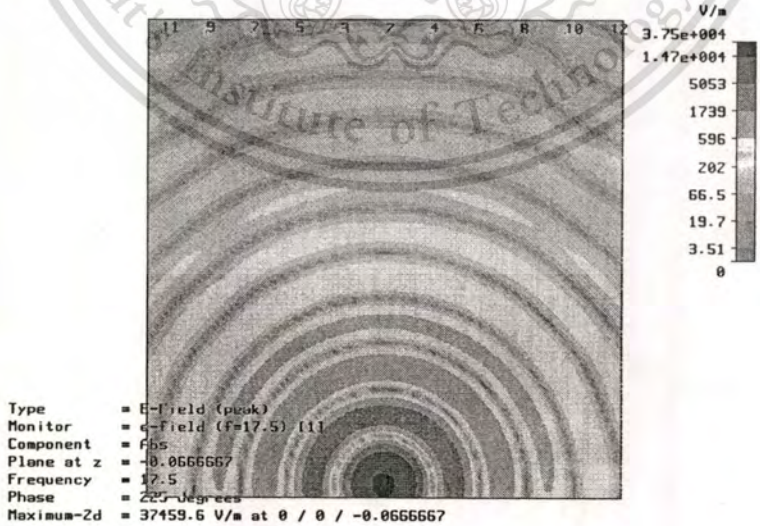

(c)

Fig. 5.2 Simulated 2D of E-field of dipole antenna array when the number of elements are (a) 2 (b) 11 (c) 20

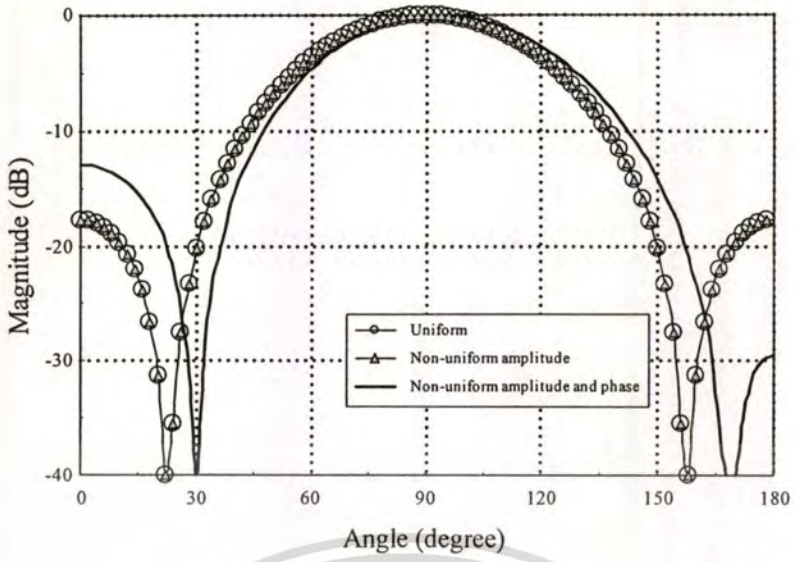

Fig. 5.3 Radiation patterns of two- element quasi-optical antenna-mixer

be noted that when the number of elements is increased, the non-uniform plane wave increases. These results show that the amplitude excitations agree with the proposed formulations (5.7 and 5.9). However, there are some errors in term of delayed phase excitation because the proposed formulations (5.8 and 5.10) ignore mutual coupling and diffraction effects. By using Table 5.1 for amplitude and phase excitation, the main beam squints and SLL errors phenomena can be illustrated by normalizing H-plane radiation patterns in Figs. 5.3, 5.4 and 5.5, respectively. Fig. 5.3 shows the H-plane radiation pattern in case of two-element quasi-optical antenna mixer for verifying the proposed formulations. The results show that the pattern of the uniform excitation is same as that of the non-uniform amplitude excitation. The non-uniform amplitude and phase excited array has the maximum of the main beam squint from 90^o (boresight) to 94^o. It occurs from the delayed phase excitation in (5.10). The comparisons of SLL of the eleven-element and twenty-element array are shown in Fig. 5.4 and 5.5.

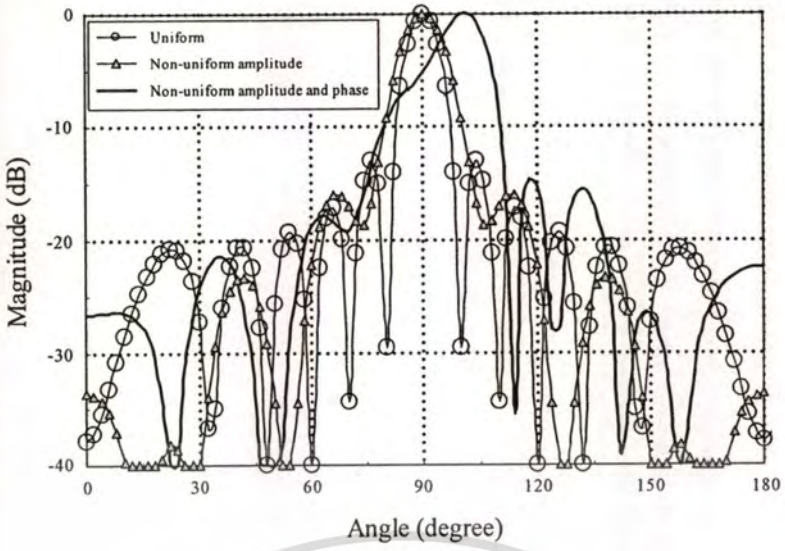

Fig. 5.4 Radiation patterns of eleven- element quasi-optical antenna-mixer

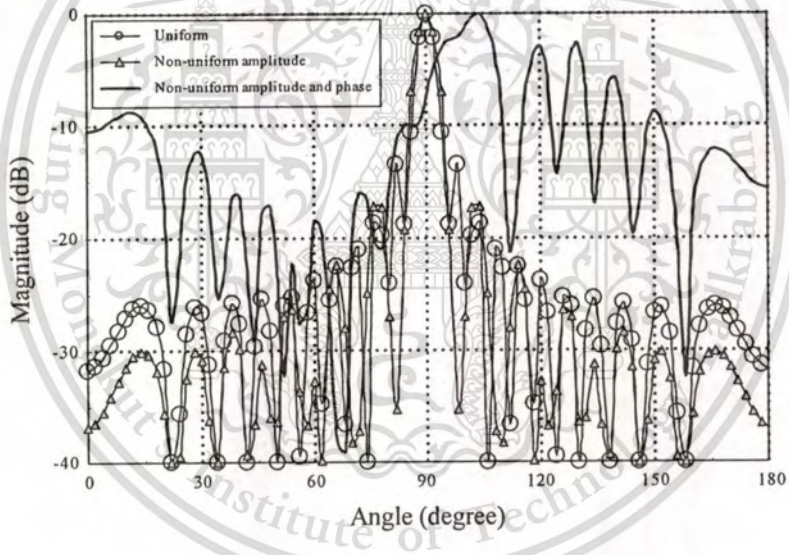

Fig. 5.5 Radiation patterns of twenty- element quasi-optical antenna-mixer

Fig 5.4 shows that by taking non-uniform amplitude and phase into account, in the eleven-element quasi-optical antenna-mixers, the shape of radiation pattern is significantly different from the one predicted by the uniform excitation. The main beam is squinted by 10^{o}. For the larger number of elements, the effect of amplitude and phase error is more pronounced. The patterns of the twenty-element array in Fig. 5.5 show the drastically different shape of the pattern, particularly the high side lobe

level (SLL). For comparison purpose, let us define the mainbeam error and SLL error as follows.

$$Mainbeam\ error = Mainbeam\ direction\big|_{Uniform} - Mainbeam\ direction\big|_{\substack{Non\text{-}uniform \\ amplitude\ and\ phase}} (degree) \tag{5.11}$$

$$SLL\ error = SLL\big|_{Uniform} - SLL\big|_{\substack{Non\text{-}uniform \\ amplitude\ and\ phase}} (\text{dB}) \tag{5.12}$$

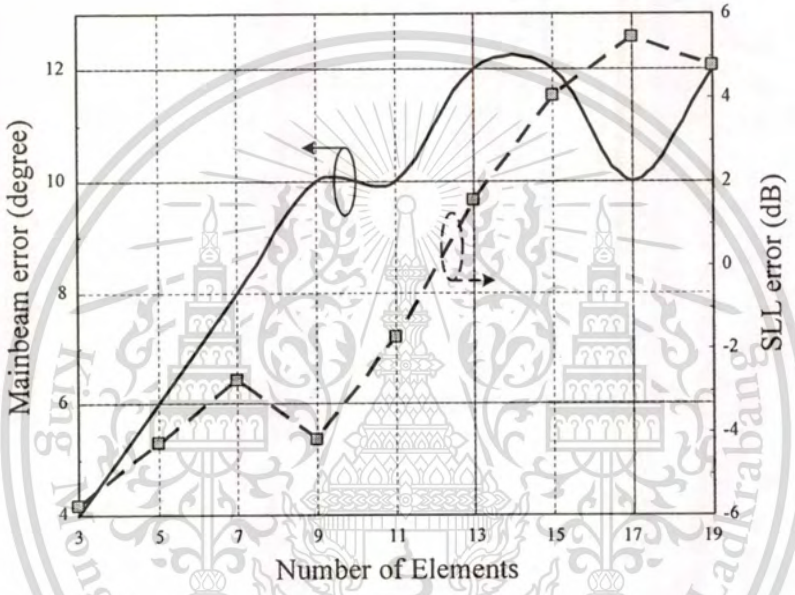

Fig. 5.6 Mainbeam and SLL error versus number of elements (Odd)

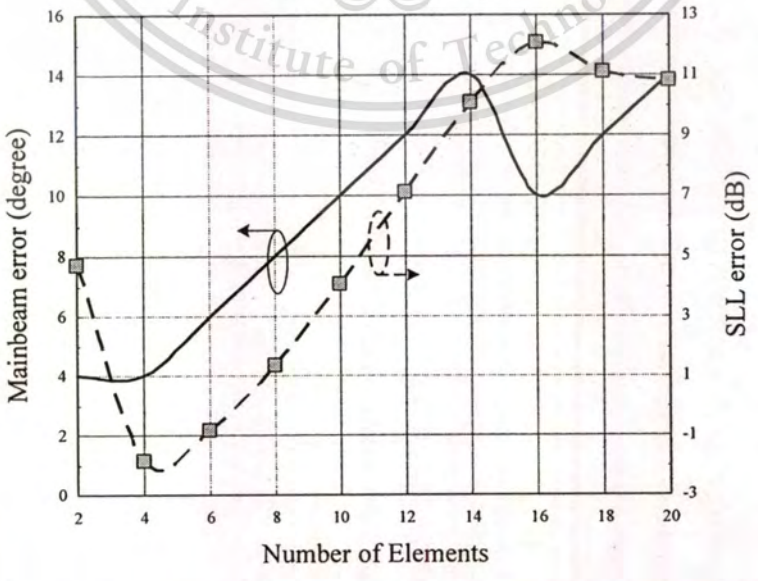

Fig. 5.7 Mainbeam and SLL error versus number of elements (Even)

Fig. 5.6 shows the main beam squint (error) increasing from 4 to 13 degrees when the number of elements increases from 3 to 19 elements. The SLL error increases almost monotonically with the number of elements are higher than 11 elements but decreasing when the number of elements. In the same manner, Fig. 5.6 shows the main beam squint (error) increases from 4 to 14 degrees when the numbers of elements increase from 2 to 20 elements, and the SLL error increasing when the numbers of elements are higher than 8 elements. It decreases when the numbers of elements are less than 6 elements. It should be noted that the SLL of the quasi-optical antenna-mixer array excited by non-uniform plane wave reduces when the number of elements are 4 and 9.

5.4 Effect of LO feeding separation

To demonstrate the effect of LO feeding antenna separation on radiation pattern, the distances are varied in case of $10D^2/\lambda$, $20D^2/\lambda$ and $30D^2/\lambda$. The antenna has four elements with distance between antenna-mixer of 0.5λ. These effects are illustrated in Fig. 5.8. The result shows the main beams squint and SLL error decreasing when the separation of LO feeding antenna increases from $10D^2/\lambda$ to $30D^2/\lambda$. These effects must be taken into account for increasing accuracy in radiation pattern prediction.

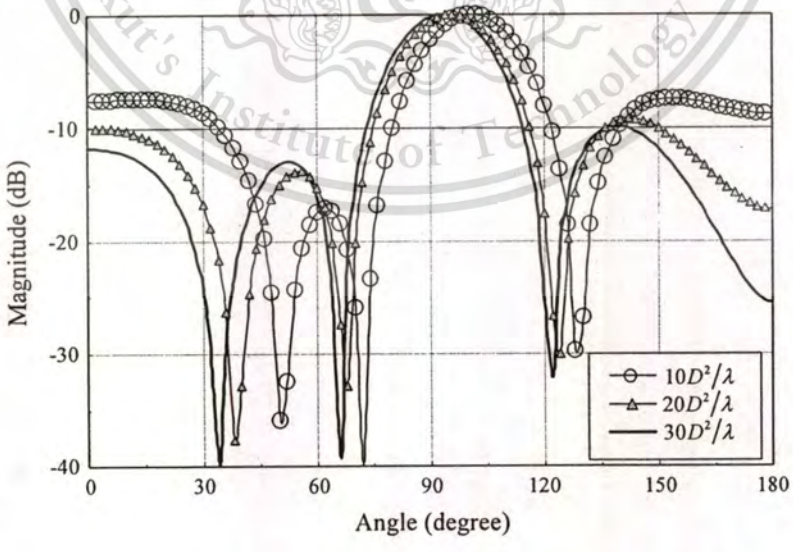

Fig. 5.8 Effect of LO feeding separation on receiving radiation pattern

5.5 Conclusion

The effect of non-uniform plane wave excited to the quasi-optical antenna-mixer array for receiving application is investigated in this work. The simulated results show the squinted mainbeam and SLL error in term of elements from of 2 to 20 elements. The SLL level of the quasi-optical antenna-mixer array is reduced when using 6 and 11 elements. The proposed formulation is used to improve radiation pattern accuracy. The LO feeding antenna separation should be increased for reducing non-uniform amplitude and phase excitation. These formulations will be applied to calibrate the amplitude and phase of the measured signal in an inverse measurement technique by using quasi-optical antenna-mixer for dielectric property determination. It will be shown in chapter 6.

CHAPTER 6
AN INVERSE TECHNIQUE IN SPATIAL DOMAIN USING QUASI-OPTICAL ANTENNA-MIXERS FOR DIELECTRIC PROPERTIES DETERMINATION

6.1 Introduction

An inverse measurement system by reflection measurement in spatial domain at 19 GHz band is implemented and tested in this chapter. Hybrid ring quasi-optical antenna-mixers, with features of high LO/RF isolation and local oscillators' synchronization, are used as probes for measuring reflected wave from the unknown object. Calibration process is proposed for accurate results. Comparison of dielectric properties of Agar phantom measured by this system with those from the commercial dielectric probe show that the error is less than 11%. It shows the potential to design a low cost dielectric-property determination system.

6.2 System Principle

An inverse technique is a procedure for determining unknown dielectric properties of a medium. It is accomplished by using optimization techniques by which performance functions are approximated. Then, parameters of the performance functions are adapted to minimize error between desired function and approximated function in the domain of independent variables. In this context, the desired function is the measured data while the approximated function is the calculated data. When multiple probes are used, loss in feeding network must be taken into account. The problem of transmission loss can be mitigated by down converting the signal to the lower frequency. However, local oscillators' synchronization is necessary when multiple receivers are used for down conversion. Quasi-optical antenna mixer has been proposed for beam scanning without phase shifters so that low loss can be accomplished at high frequency. Using one local oscillator, intermediate frequency from each element of the mixer antenna can be simply measured.

An inverse measurement technique in spatial domain [23] using quasi-optical antenna mixers transmits a single continuous wave from a transmitter (Tx) toward a target. Then N antennas are used to receive reflected wave from the target. Output from the antennas will be complexly measured for amplitude and phase, respectively. Since signal processing at high frequency is not convenient due to loss, these signals are down converted to intermediate frequency (IF) signal. Then these complex reflected IF signals will be fed to the inverse technique algorithm based on steepest descent method to iteratively minimize error between measured and calculated waves to find unknown ε_r' and ε_r'' of the target. The diagram of the proposed system is shown in Fig. 6.1.

Let assume that a plane wave of amplitude E_0 is obliquely incident from a free space of propagation constant k_0 onto an infinite half plane of homogenous lossy dielectric medium with angle θ_i as shown in Fig. 6.1. To simplify the calculation, homogeneous dielectric half space is considered. In addition, mutual coupling between the antenna elements are neglected.

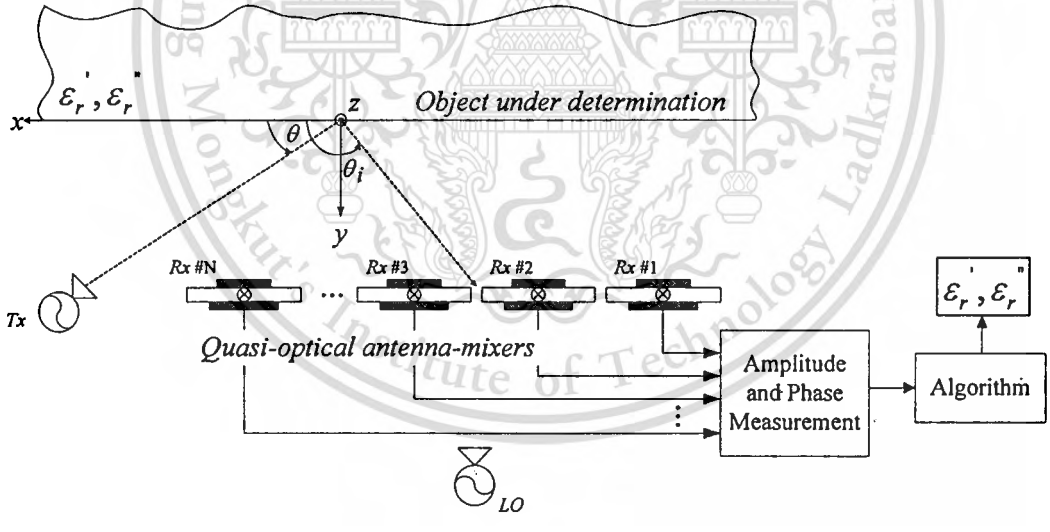

Fig.6.1 Block diagram of the proposed system

Reflected waves from obliquely incident wave at an observation point $P(r,\theta)$ can be considered in case of the perpendicular and parallel polarization [23]. Since microstrip antennas will be used as probes and exhibit vertical polarization, hence perpendicular polarization case is considered. The reflected wave $\bar{E}_\perp^r$ is

$$\bar{E}_{\perp}^{r} = \hat{a}_z R_{\perp} E_0 e^{jk_0 r\cos(\theta+\theta_i)} \tag{6.1}$$

where $R_{\perp}$ is a reflection coefficient of the lossy dielectric medium in the case of perpendicular polarization. Reflection coefficient is given by [23]

$$R_{\perp}(\theta) = \frac{\sin\theta - \sqrt{\varepsilon_r - \cos^2\theta}}{\sin\theta + \sqrt{\varepsilon_r - \cos^2\theta}} \tag{6.2}$$

where ε_r is the complex relative permittivity of the lossy dielectric medium, which is a function of dielectric constant (ε_r') and loss factor (ε_r''). The loss factor is equal to $\sigma / \omega\varepsilon_o$, where σ is the conductivity, ω is angular frequency and ε_o is the permittivity of free space. The complex relative permittivity is defined as

$$\varepsilon_r = \varepsilon_r' - j\varepsilon_r'' \tag{6.3}$$

A number of optimization techniques have been developed. There are many performance functions depended upon the problem as mentioned in [24] where the square of performance functions increases error of parameter vectors rapidly. In this work, the suitable performance functions are the summation of absolute of difference between measured and calculated quantities, e.g. real and imaginary parts of the reflected waves. Measured results ($\bar{E}_{Meas}^{r}$) are obtained from measurement while calculated ones ($\bar{E}_{Cal}^{r}$) are obtained from (6.1) to (6.3). Therefore, the performance functions, Q_1 and Q_2, can be expressed mathematically as

$$Q_1(\bar{X},\omega_j) = \sum_{j=1}^{L}\left|\left[\mathrm{Re}\left[\bar{E}_{Meas}^{r}(\omega_j)\right] - \mathrm{Re}\left[\bar{E}_{Cal}^{r}(\bar{X},\omega_j)\right]\right]\right| \tag{6.4}$$

$$Q_2(\bar{X},\omega_j) = \sum_{j=1}^{L}\left|\left[\mathrm{Im}\left[\bar{E}_{Meas}^{r}(\omega_j)\right] - \mathrm{Im}\left[\bar{E}_{Cal}^{r}(\bar{X},\omega_j)\right]\right]\right| \tag{6.5}$$

where $\bar{X}$ is a parameter vector (i.e., ε_r' and ε_r'') and ω_j is j^{th} independent variable of L sampling points. In this paper, ω_j is the measurement position. The total performance function is a summation of each performance function that can simultaneously be optimized. It is defined as

$$Q(\bar{X},\omega_j)=Q_1(\bar{X},\omega_j)+Q_2(\bar{X},\omega_j). \tag{6.6}$$

The performance function can be optimized to find the minimum function. The first order derivative of the function at any point represents the direction of the maximum increment of the function value. Thus, minimum function value should be searched along the opposite direction of the first order derivative direction. It is called a descent search direction, which is defined as

$$\bar{d}=-\nabla Q(\bar{X},\omega_j). \tag{6.7}$$

The condition $\max_{\bar{d}} \delta$ is solved by using the linear programming that satisfies the condition $-\nabla Q^T(\bar{X},\omega_j)\cdot\bar{d}\geq\delta$ and $0\leq\|\bar{d}\|\leq 1$, where the superscript T is the transpose of the matrix and $\|\cdot\|$ is the norm of the matrix. In case of $\delta\leq 0$, an error occurs and the calculation is terminated. Initial values and performance functions should be changed and calculation is restarted. In the case of $\delta>0$, the calculation continues and the step length α^* is defined as a positive value that found among each performance function by using the bounding phase method and golden section search calculation. The parameter vector is calculated from the descent search direction and the step length that has been adapted. If the performance function of the parameter vector is greater than the former one, then α^* is decreased to an appropriate value and the parameter vector is recalculated. If performance function from the parameter vector is less than the former one, then program continues the calculation in the next iteration loop until the error (performance function) is less than a specified tolerance or the relative change of error is constant value. Then, the parameter vectors at this step are acceptable values.

6.3 Effect of RF/LO isolation on IF error

Generally, the reflected RF signal is delivered to the mixers at the upper ports whereas the LO signal from the LO oscillator is delivered to the lower ports. Then, IF signals are measured at outputs of the mixers. The accuracy of the system depends on the accurate measured IF signals for inverse calculation to obtain unknown dielectric property. If the object under determination reflected the LO retransmission signal and entered the upper ports, for simplicity, assume that the reflection of the retransmission can be C times of the LO signal $(0 \le C \le 1)$ with phase shift of $D(-180^o \le D \le 180^o)$. There will be other LO signal $(C\cos(\omega_{LO}t + D))$ entering the upper ports of the quasi-optical antenna-mixers. The output IF signals of the mixer are

$$IF = \frac{1}{2}\left[\begin{array}{l}\cos(\omega_{RF}t + \omega_{LO}t) + \cos(\omega_{RF}t - \omega_{LO}t) + \\ C\cos(\omega_{RF}t + \omega_{LO}t + D) + C\cos(\omega_{RF}t - \omega_{LO}t - D)\end{array}\right]. \qquad (6.8)$$

By filtering the RF, LO and up converted signals out, the down converted signals becomes

$$IF = \frac{1}{2}\left[\cos(\omega_{RF}t - \omega_{LO}t) + C\cos(\omega_{RF}t - \omega_{LO}t - D)\right]. \qquad (6.9)$$

The ideal output signal of those in Equation (6.9) is the first term when C and D are zero, otherwise it will be different and results in error. The error can be defined by

$$Error(\%) = \frac{Eq.(6.9)\big|_{C=D=0} - Eq.(6.9)\big|_{arbitrary\ C,D}}{Eq.(6.9)\big|_{C=D=0}} \times 100. \qquad (6.10)$$

To illustrate effect of LO retransmission on output signal error, Table 6.1 shows the error for different C and D (worst case). The error is 0% when C is 0 (no LO retransmission) and is 100% for total LO retransmission from the object. The lower values of C corresponding to low LO retransmission provide less error of the IF signal. This error has a significant effect on inverse measurement technique for dielectric property determination [23]-[24] which complex IF signals are measured at

the IF port. The LO retransmission should be less than 10dB to provide less error than 10%.

Table 6.1 Error for different C's and D's

C (Isolation dB)	1 (0 dB)	0.1 (10 dB)	0.001 (20 dB)	0.0 (∞ dB)
D	$0,180^o$	$0,180^o$	$0,180^o$	$0,180^o$
Error (%)	100	10	2	0

6.4 System design and measurement results

A quasi-optical antenna-mixer, which the radio frequency (RF) and the local oscillator (LO) signals are transformed to the intermediate frequency (IF) at the antenna, was proposed to resolve transmission line loss. LO to RF isolation was increased by using a hybrid ring coupler that were analyzed and designed in chapter 3. Measured results show that this quasi-optical antenna-mixer provide RF/LO isolation better than 29dB at 18.19GHz. Therefore, this chapter demonstrates these quasi-optical antenna-mixers for picking up the reflected signal. The system is demonstrated at 19.3GHz to measure dielectric properties of Agar phantom. Two quasi-optical antenna mixers are used as probes and arranged in vertical polarization as a photograph in Fig. 6.2. Two HP-P281C waveguide to coaxial adaptors were used to transmit RF and LO signals. One was connected to an HP 83640B Signal Generator to transmit RF signal at 19.3GHz. The other is connected to an Agilent 83630B to transmit 18.3GHz of LO signal. The LO antenna is located at 70mm away from the middle of antenna-mixers. The RF transmitting antenna is located with 70^o (θ in Fig. 6.1) from the normal direction of the Agar phantom at the distance of 130mm from the antenna-mixers. An object under test is a 300x300x10mm^3 Agar phantom which is 180mm from the antenna-mixers. It is prepared by mixing Agar powder with 956.6*cc* of distilled water at 80^oC, 2.4*gm* of NaCl and 1.0*gm* of NaN_3. Dielectric properties of Agar phantom can be varied by varying quantity of Agar powder. The dielectric constant is inversely proportional to Agar powder. The experiments were performed with Agar phantoms which have relative permittivity ε_r of $29.36 - j21.08$ and $39.19 - j31.86$. The environmental setup was covered by Emerson AN-77 absorbers.

Complex reflected wave from the Agar phantom was measured by using a Tektronix TDS 3032 oscilloscope and fed to the optimization algorithm. Before data acquisition process, the magnitudes and phases of IF signals have to be compensated (or hardware calibration) by placing the RF transmitting antenna in front, at the middle point, of the quasi-optical antenna-mixers. The amplitude was calibrated by adjusting the biasing mixer-diodes currents. However, the phase calibration cannot be adjusted directly. It was accomplished by measuring the IF signals as shown in Fig. 6.3 and taking into account in the optimization algorithm. This phase difference is due to non-linear effect of diode-mixer.

For software calibration process, the calculated results are based on uniform plane wave assumption, however the LO transmitted wave is illuminated by an open-end waveguide with non-uniform pattern. Hence, calibration of amplitude and phase must be accomplished. The amplitude can be calibrated by H-plane radiation pattern of the TE_{10}-mode [30] as

$$A_{(n)} = -\frac{\pi}{2} C \cos(\theta_n) \cos\phi \frac{\cos X}{X^2 - \left(\frac{\pi}{2}\right)^2} \frac{\sin Y}{Y} \tag{6.11}$$

where

$$C = j\frac{abkE_0 e^{-jkr}}{2\pi r}, \tag{6.12}$$

$$X = \frac{ka}{2}\sin\theta\cos\phi, \tag{6.13}$$

and

$$Y = \frac{kb}{2}\sin\theta\sin\phi. \tag{6.14}$$

The normalized amplitude compensation of H-plane TE_{10}-mode becomes

$$A_{(n)} = -0.25abke^{-jkr}\cos(\theta_n)\frac{\cos\left(\frac{ka}{2}\sin(\theta_n)\right)}{\left(\frac{ka}{2}\sin(\theta_n)\right)^2 - \left(\frac{\pi}{2}\right)^2} \tag{6.15}$$

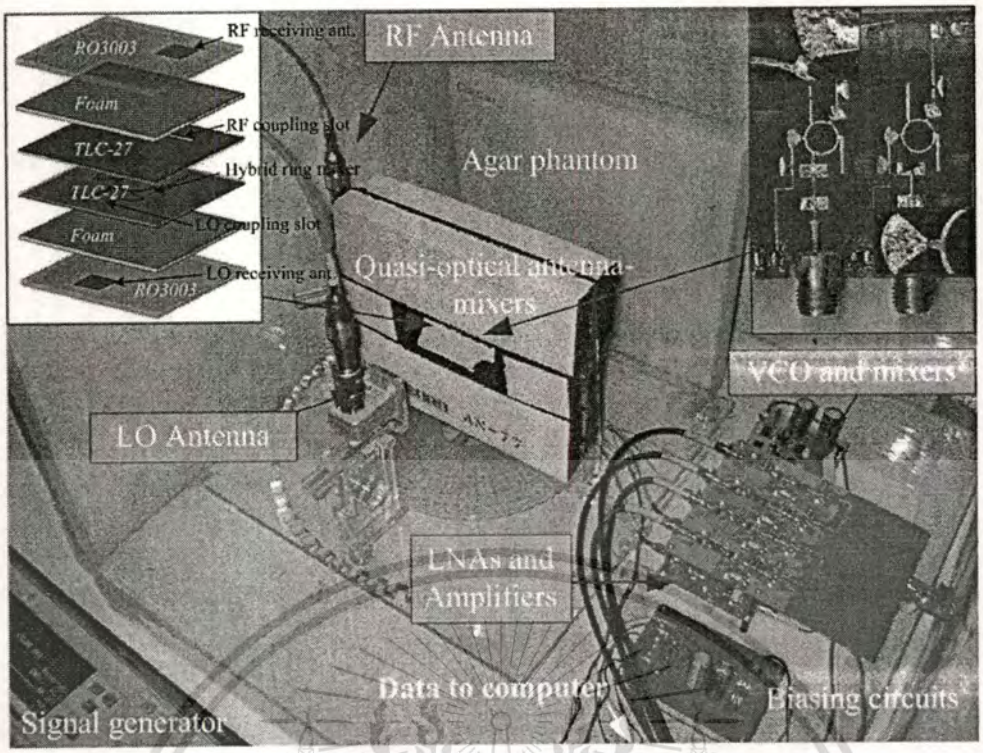

Fig. 6.2 Photograph of the system

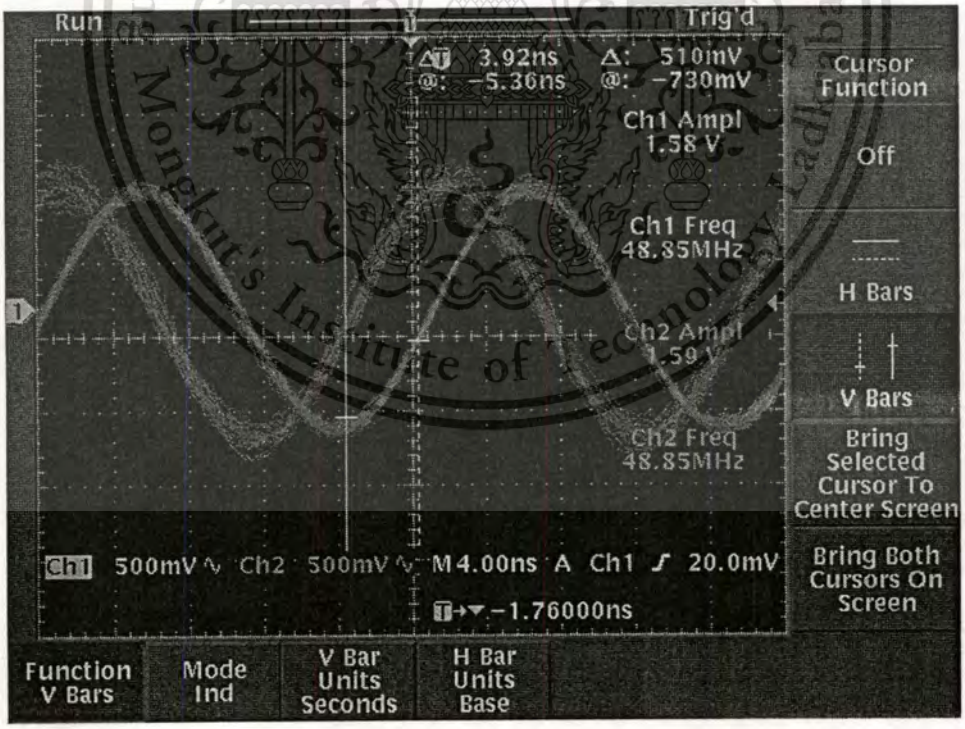

Fig. 6.3 Calibrated IF signal amplitudes before data acquisition process

where

$$\theta_n = \tan^{-1}\left(\frac{\frac{2n-1}{2}d}{r}\right) \tag{6.16}$$

a is waveguide aperture length, b is waveguide aperture width, r is the distance between LO transmitting antenna to quasi-optical antenna-mixer, d is separation between quasi-optical antenna-mixers (0.9λ) and k is wave number. The received RF signal is transformed to IF signal at each array element. The non-uniform LO amplitude and phase excitation can be determined from the different propagation paths from the LO transmitting antenna to each element of the array. Using the relationship of plane wave and the spherical wave at the observation point, phase can be calibrated by using the assumption for compensating formulations as shown in Fig. 6.4.

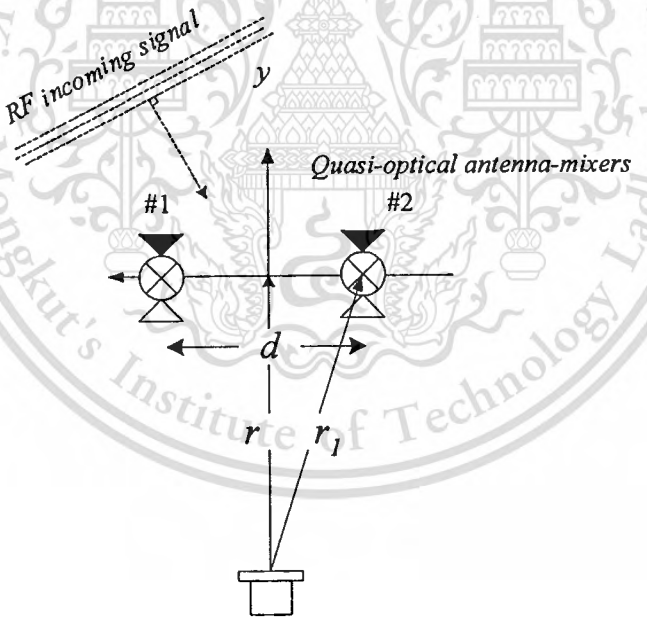

Fig. 6.4 Calibration process

Referring to Fig. 6.4, the non-uniform LO amplitude and phase excitation can be determined from the different propagation paths from the LO transmitting antenna to each element of the array. The free space loss and phase shift are different. The

amplitude and phase excitation of each array element for the array can be expressed in (6.17) and (6.18), respectively.

$$A_{L(2elements)} = \frac{r}{\sqrt{(0.5d)^2 + r}} \tag{6.17}$$

$$\phi_{L(2elements)} = k\left[\sqrt{r^2 + (0.5d)^2} - r\right] \tag{6.18}$$

where r and d are the distance between the LO transmitting antenna to the quasi-optical antenna-mixers (far-field region) and the separation between antenna-mixer elements, respectively. ϕ_o is an initial phase at the center of the n^{th} element, and k is the wave number. Note that in this investigation, two elements were used. The un-calibrated and calibrated reflected waves of different Agar phantoms are illustrated in Table 6.2 and 6.3. The relative permittivity (ε_r'(inv.) and ε_r''(inv.)) in case of un-calibrated and calibrated reflected waves compared with the relative permittivity obtained by using a dielectric probe [40] are illustrated.

Table 6.2 Relative permittivity in case of un-calibrated waves

	Magnitude (V)		Phase (degrees)		ε_r' (inv.)	ε_r'' (inv.)	ε_r' (probe)	ε_r'' (probe)	Number of iterations	% error	
	Ch1	Ch2	Ch1	Ch2						ε_r'	ε_r''
Sample1	1.19	1.15	00.00	96.05	32.94	25.38	29.36	21.08	46,000	12.2	20.4
Sample2	1.03	0.91	00.00	97.00	45.30	39.21	39.19	31.86	34,000	15.6	23.1

Table 6.3 Relative permittivity in case of calibrated reflected waves

	Magnitude (V)		Phase (degrees)		ε_r' (inv.)	ε_r'' (inv.)	ε_r' (probe)	ε_r'' (probe)	Number of iterations	% error	
	Ch1	Ch2	Ch1	Ch2						ε_r'	ε_r''
Sample1	0.94	0.90	00.00	67.69	31.85	23.12	29.36	21.08	20,000	8.5	9.7
Sample2	0.78	0.66	00.00	68.63	42.91	35.11	39.19	31.86	18,000	9.5	10.2

The results show that the number of iterations (calculation time) and % error are reduced when using the proposed calibration process. The main cause of error is due to finite size of sample in measurement which calculation is accomplished from the assumption of infinite half space.

6.4 Conclusion

This chapter shows the dielectric property determination of lossy medium by an inverse technique, which can be implemented in spatial domain by using quasi-optical antenna mixers. The system was validated by implementation of two antennas to measure dielectric of unknown object. The proposed calibration process provides accurate results with error between the proposed system and the dielectric probe is less than 11%. The system is useful in non-destructive dielectric property determination.

CHAPTER 7
CONCLUSIONS AND DISCUSSIONS

This thesis presents a study on characteristics of a quasi-optical antenna-mixer and its applications. To eliminate the transmission line losses of the conventional receiver, the quasi-optical antenna-mixer is used as a mixer in the receiver. Therefore, it has no losses because of any used transmission line or high frequency circuits such as phase shifter circuits are not needed. To provide a beam scanning antenna, it can be accomplished by using quasi-optical antenna-mixers fed by LO transmitting antenna. The mainbeam is controlled by moving LO transmitting direction or adjusting LO frequency.

In chapter 2, the fundamental of quasi-optical antenna-mixer and the theoretical background for beam scanning system using this antenna are described and analyzed. The beam scanning scheme is divided into two means. One is changing the LO transmitting frequency. The other is moving LO transmitting direction. The calculated results show that the receiving IF signal direction is sensitive to the LO transmitting antenna direction, and the scanning mainbeam capabilities are critically limited by the frequency ratio. For accurate mainbeam prediction, the distance between RF and LO receiving antenna ratio should be the same. The limit of RF scan directions is 0 to 180 degrees of all directions by using higher LO frequency than RF frequency. Furthermore, the scanning mainbeam capabilities are critically limited with the frequency ratio.

The high RF/LO isolation of quasi-optical antenna called a hybrid ring quasi-optical antenna-mixer, with analysis and design, is presented in chapter 3. The hybrid ring singly balance mixer, feeding with a back-to-back aperture coupled inverted square patch, is used for RF to LO isolation improvement. It was analyzed and found that a hybrid ring radius has a sensitive effect on RF/LO isolation. A slot length should be longer than a patch width to obtain wide bandwidth. This antenna provides significant RF/LO isolation compared with the conventional ones. It provides around 29dB RF/LO isolation and 16dB conversion loss with 4.37% frequency shift from the desired frequency. The isotropic conversion loss can be improved by utilizing the load-pull technique.

In chapter 4, a multibeam antenna using quasi-optical antenna-mixers is presented. The accurate RF receiving mainbeam direction can be obtained when the element pattern is taken into account. The three beam demonstration simultaneously is achieved by using three LO transmitters. It can be used in multibeam operation, and this antenna can be designed without using a complicated feeding system by using quasi-optical antenna-mixers. The effect due to non uniform of radiation pattern of antenna element multiplication is illustrated. The effectiveness of a three-beam antenna is demonstrated at K-band showing accurate beam directions which is very useful in modern wireless communications.

Chapter 5 illustrates the effect of non-uniform plane wave on radiation pattern of a quasi-optical antenna mixer array. The calculated results show that non-uniform plane wave effects on beam squint and SLL error. It is predicted in term of magnitude and phase excitation that are derived in odd and even cases. The proposed formulations, verify by compared with CST2006^{TM} simulator, are used to improve radiation pattern accuracy and to calibrate magnitude and phase for inverse technique.

Chapter 6 presents a dielectric property determination by an inverse technique which can be implemented in spatial domain by using quasi-optical antenna mixers. The system was validated by implementation of two antennas to measure dielectric of agar phantom. The calibration process including hardware and software provide accurate results with error compared with the commercial dielectric probe are less than 11%.

This thesis has presented the full design, development and test results of the quasi-optical antenna-mixer. Its application has been demonstrated in a number of practical examples. However, there are many other interesting areas in which this antenna can be usefully applied. With respect to these new areas, further work may be required with regard to such issues as miniaturization of the hybrid ring size [38] for reducing SLL.

REFERENCES

[1] L. Yuan, J. Paul and P. Yen, "140GHz quasi-optical planar mixer," *IEEE MTT-S Digest.*, pp. 374-375, 1982.

[2] K. D. Stephan, N. Camilleri and T. Itoh, "A quasi-optical polarization-duplexed balanced mixer for millimeter-wave applications," *IEEE Trans. Microwave Theory and Techniques*, vol. MTT-31, no. 2, pp. 164–170, Feb. 1983.

[3] K. D. Stephan and T. Itoh, "A planar quasi-optical subharmonically pumped mixer characterized by isotropic conversion loss," *IEEE Trans. Microwave Theory and Techniques*, vol. MTT-32, no. 1, pp. 97-102, Jan. 1984.

[4] V. D. Hwang , T. Uwano and T. Itoh, "Quasi-optical integrated antenna and receiver front end," *IEEE Trans. Microwave Theory and Techniques,* vol. 36, no. 1, pp .80-85, Jan. 1988.

[5] V. D. Hwang and T. Itoh, "Quasi-optical HEMT and MESFET self-oscillating mixers," *IEEE Trans. Microwave Theory and Techniques*, vol. 36, no. 12, pp. 1701-1705, Dec. 1988.

[6] S. K. Masarweh, T. N. Sherer, K. S. Yngvesson, "Modeling of a monolithic slot ring quasi-optical mixer," *IEEE Trans. Microwave Theory and Techniques*, vol. 42, no. 9, pp. 1602–1609, Sep. 1994.

[7] C. Y. Tong and R. Bludell, "A self-diplexing quasi-optical magic slot balanced mixer," *IEEE Trans. Microwave Theory and Techniques,* vol. 42, no. 3, pp. 383–388, Mar. 1994.

[8] S. V. Robertson and L. P. B. Katehi, "A planar quasi-optical mixer using a folded-slot antenna," *IEEE Trans. Microwave Theory and Techniques*, vol. 43, no. 4, pp. 896-898, Apr. 1995.

[9] D Neculoiu, G Bartolucci, *et al.*, "A micromachined 38GHz schottky-diode uniplanar monolithic integrated quasi-optical mixer," *IEEE Radio Frequency Integrated Circuits (RFIC) Symposium*, pp. 531–534, 2004.

[10] L. Waddinger and V. Nalbandian, "Millimeter-wave power combiner using quasi-optical techniques," *IEEE Trans. Microwave Theory and Techniques*, vol. 83, no. 2, pp. 189-193, Feb. 1983.

[11] W. J. Mink, "Quasi-optical power combining of solid-state millimeter-wave sources," *IEEE Trans. Microwave Theory and Techniques*, vol. MTT-34, no. 2, pp. 273-279, Feb. 1986.

[12] R. A. York and R. C. Compton, "Quasi-optical power combining using mutually synchronized oscillator arrays," *IEEE Trans. Microwave Theory and Techniques*, vol. 39, no. 6, pp. 1000-1009, Jun. 1991.

[13] J. Birkeland and T. Itoh, "A 16 element quasi-optical oscillator power combining array with external injection locking," *IEEE Trans. Microwave Theory and Techniques*, vol. 40, no. 3, pp. 475-481, Mar. 1992.

[14] W. Leverich, X. Wu and K. Chang, "FET active slotline notch antennas for quasi-optical power combining," *IEEE Trans. Microwave Theory and Techniques,* vol. 41, no. 9, pp. 1515-1518, Sep. 1993.

[15] X. W. Wu and K. Chang, "Novel active FET circular patch antenna arrays for quasi-optical power combining," *IEEE Trans. Microwave Theory and Techniques*, vol. 42, no. 5, pp. 766-771, May 1994.

[16] J. Lin and T. Itoh, "Two-dimensional quasi-optical power-combining arrays using strongly coupled oscillators," *IEEE Trans. Microwave Theory and Techniques*, vol. 42, no. 4, pp. 734-741, Apr. 1994.

[17] C. Chi and M. Rebeiz, "A quasi-optical amplifier," *IEEE Microwave and Guided Wave Letters*, vol. 3, no. 6, pp. 164-166, Jun. 1993.

[18] N. J. Kolias and R. C. Compton, "A microstrip-based unit cell for quasi-optical amplifier arrays," *IEEE Microwave and Guided Wave Letters*, vol. 3, no. 9, pp. 330-332, Sep. 1993.

[19] T. P. Budka, M. W. Trippe, S. Weinreb and G. M. Rebeiz, "A 75GHz to 115GHz quasi-optical amplifier," *IEEE Trans. Microwave Theory and Techniques,* vol. 42, no. 5, pp. 899-901, May 1994.

[20] J. Schoenberg, T. Mader, B. Shaw and Z. B. Popovic, "Quasi-optical antenna array amplifiers," *IEEE MIT-S Digest.,* pp.605-608, 1995.

[21] T. Nishimura, N. Ishii and K. Itoh, "Beam scan using the quasi-optical antenna mixer array," *IEEE Trans. Antennas and Propagation,* vol. 47, no. 7, pp. 1160-1166, July 1999.

[22] H. Saito, T. Nishimura, M. Yamamoto and K. Itoh, "Quasi-optical antenna-mixer array composed of a magnetic loop antenna operated at 10-GHz band," *Electronics and Communications in Japan 2004*; vol. 87, no. 4, pp. 45-53.

[23] K. P. Thakur and W. S. Holmes, "Noncontact measurement of moisture in layered dielectrics from microwave reflection spectroscopy using an inverse technique," *IEEE Trans. Microwave Theory and Techniques,* vol. 52, no.1, pp.76-82, Jan. 2004.

[24] J. Park and C. Nguyen, "An ultrawide-band microwave radar sensor for nondestructive evaluation of pavement subsurface," *IEEE Sensors Journal*, vol. 5, no. 5, pp. 942-949, Oct. 2005.

[25] J. Mearnchu, D. Torrungrueng, C. Phongcharoenpanich and M. Krairiksh, "An inverse technique for dielectric-property determination from reflection measurement in spatial domain," *Proc. of APMC 2005*, China, vol.5, pp. 3051-3054.

[26] J. Paulraj, D. Gore, R. Nabar and H. Bolcskei, "An overview of MIMO communications - A key to gigabit wireless" *Proceedings of the IEEE 2004*, vol. 92, pp.198-18.

[27] G. Foschini and M. Gans, "On limits of wireless communications in a fading environment when using multiple antennas," *Wireless Personal Communications 1998*, vol. 6, pp. 311-35.

[28] P. Perini and C. Holloway, "Angle and space diversity comparisons in different mobile radio environments," *IEEE Trans. Antennas and Propagation*, vol. 46, no. 6, pp. 764-775, Jun. 1998.

[29] D. M. Pozar, *Microwave Engineering*: New York: John Wiley & Sons, 1998.

[30] C. A. Balanis, *Antenna Theory: Antenna theory analysis and design*. 2nd ed. New York: John Wiley & Sons, 1997.

[31] J. F. Zurcher and F. E. Gardiol, *Broadband patch antennas:* Norwood, MA: Artech House, 1995.

[32] Advanced Design System Fundamentals. Agilent EEsof EDA. Part Number E89 00-90329-ADS 1.5 (4/01).

[33] CST Microwave Studio® 3D EM for High Frequency. CST STUDIO SUITE™ 2006.

[34] D. Le and F. M. Ghannouchi, "Multitone characterization and design of FET resistive mixers based on combined active source–pull/load–pull techniques," *IEEE Trans. Microwave Theory and Techniques,* vol. 46, no. 9, pp. 1201-1208, Sep. 1998.

[35] A. Velazquez, A. Lazaro, L. Pradell and A. Comeron, "Application of CAD load-pull techniques in mixer design," *Microwave and Optical Technology Letters.,* vol. 36, pp. 320-323, 2003.

[36] http://www.avagotech.com/assets/downloadDocument.do?id=1811.

[37] U. L. Rohde and D. P. Newkirk, *RF/Microwave circuit design for wireless applications.* New York: John Wiley & Sons, Inc, 2000.

[38] H. Lee, K. Choi and H. Hwang, "A harmonic and size reduced ring hybrid using coupled lines," *IEEE Microwave and Wireless Components Letters.,* vol. 17, no. 4, April 2007.

[39] C. A. Balanis, *Advanced Engineering Electromagnetic*. New York: John Wiley & Sons, 1997.

[40] http://www.home.agilent.com/agilent/product.jspx?cc=US&lc=eng&nid=53690 2475.536883502&pageMode=PL.

RELATED PUBLICATIONS

1). S. Janin, K. Sripimanwat, C. Phongcharoenpanich and M. Krairiksh, "A multibeam antenna using quasi-optical hybrid ring antenna-mixer array," *Proc. of the 2005 International Technical Conference on Circuits/System, Computers and Communications (ITC-CSCC 2005)*, Korea, July 2005.

2). S. Janin, P. Dangrattanawong, K. Sripimanwat, C. Phongcharoenpanich and M. Krairiksh, "Characteristics of a multibeam antenna using quasi-optical hybrid ring antenna-mixer array," *Proc. of the 2005 Asia-Pacific Microwave Conference (APMC2005)*, Suzhou, China, vol. 5, pp. 1514-1517, Dec. 2005.

3). S. Janin, K. Sripimanwat and M. Krairiksh, "Effect of non-uniform plane wave on radiation pattern of a quasi-optical antenna-mixer array," *Proc. of the 2007 Asia-Pacific Microwave Conference (APMC2007)*, Bangkok, pp. 1135-1138, Dec. 2007

4). S. Janin, K. Sripimanwat, C. Phongcharoenpanich and M. Krairiksh, "A multibeam antenna using quasi-optical antenna-mixers," *AEU- International Journal of Electronics and Communications*, (in Press)

5). S. Janin, K. Sripimanwat, C. Phongcharoenpanich and M. Krairiksh, "A hybrid ring coupler quasi-optical antenna-mixer," *AEU- International Journal of Electronics and Communications*, (in Press).

AUTHOR BIOGRAPHY

Suwan Janin was born on June 14, 1979 in Chiang Mai, Thailand. He received the B.IT. and M.Eng. degrees in telecommunications from King Mongkut's Institute of Technology Ladkrabang, Bangkok, Thailand, in 2002 and 2004. Mr. Janin received an award from Thailand Graduate Institute of Science and Technology (TGIST) Ph.D. Program, Thailand Research Fund, during 2004 to 2007. His research area is about an antenna design for wireless applications, an RF circuit design, a quasi-optical antenna-mixer design, an array antenna and beam scanning technique.